chemistry

MDPI

Review

Recognizing New Types of Stacking Interactions by Analyzing Data in the Cambridge Structural Database

Dušan P. Malenov and Snežana D. Zarić *

University of Belgrade—Faculty of Chemistry, Studentski trg 12–16, 11000 Belgrade, Serbia
* Correspondence: szaric@chem.bg.ac.rs

Abstract: Cambridge Structural Database (CSD) is the largest repository of crystal data, containing over 1.2 million crystal structures of organic, metal–organic and organometallic compounds. It is a powerful research tool in many areas, including the extensive studying of noncovalent interactions. In this review, we show how a thorough analysis of CSD crystal data resulted in recognition of novel types of stacking interactions. Even though stacking interactions were traditionally related to aromatic systems, a number of crystallographic studies have shown that nonaromatic metal–chelate rings, as well as hydrogen-bridged rings, can also form stacking interactions. Joined efforts of a CSD analysis and quantum chemical calculations showed that these new stacking interactions are stronger than stacking interactions of aromatic species and recognized them as very important attractive forces in numerous supramolecular systems.

Keywords: noncovalent interactions; Cambridge Structural Database; crystal structures; stacking interactions; coordination compounds; chelates; hydrogen-bridged rings; RAHB; quantum chemistry

Citation: Malenov, D.P.; Zarić, S.D. Recognizing New Types of Stacking Interactions by Analyzing Data in the Cambridge Structural Database. *Chemistry* **2023**, *5*, 2513–2541. https://doi.org/10.3390/chemistry5040164

Academic Editor: Matthias Weil

Received: 22 July 2023
Revised: 19 October 2023
Accepted: 25 October 2023
Published: 13 November 2023

1. Introduction

The review titled "A Million Crystal Structures: The Whole Is Greater than the Sum of Its Parts" was published in 2019 [1], approximately at the time when the millionth crystal structure was deposited in the Cambridge Structural Database (CSD) [2]. This review described how the data from the CSD are used as a tool in the fundamental research on molecular structures and geometries, intermolecular interactions and molecular assemblies, and shows the potential for being used in industry and other commercially relevant areas [1].

One of the areas where the analysis of the data from the CSD was extensively used is the area of noncovalent interactions. One can combine the analysis of the crystal structures in the CSD with quantum chemical calculations. By analyzing the crystal structures in the CSD, one can recognize the existence of the certain types of noncovalent interactions. This includes finding the occurrence of interactions in crystal structures and describing their typical geometrical parameters. Although shorter or longer distances can indicate stronger or weaker interactions, the data from the crystal structures cannot reveal the energies of the interactions. To show that the recognized interactions are not just the consequence of crystal packing and other surrounding interactions in the crystal environment, the calculations are performed on a very high CCSD(T)/CBS level to obtain very accurate interaction energies, which can then be compared for various systems.

Using this methodology, we were able to recognize several new types of noncovalent interactions [3–11]. In this review, we focus on new types of stacking interactions. Stacking interactions are very important in many chemical and biological systems, starting from the DNA [12] and protein structure [13], and finding their application in areas such as drug design [14], crystal engineering [15] and materials science [16]. Although traditionally related to organic aromatic systems, stacking interaction exists and can be quite strong in nonaromatic systems as well. In this paper, we will summarize our findings on stacking

interactions of metal–chelate rings and hydrogen-bridged rings based on thorough studies of CSD crystal structures and quantum chemical calculations.

2. Stacking Interactions of Chelate Rings

Until the beginning of the 21st century, it was common to consider stacking interactions a feature of aromatic molecules. The typical aromatic system for studying stacking interactions is the dimer of benzene. Plenty of theoretical work was performed with the aim of elucidating the geometries of various dimers of benzene, as well as their energies [17–20]. The strongest stacking interaction is a minimum on the potential energy surface for the benzene dimer (Figure 1); it has a displaced–stacked geometry with a horizontal displacement of 1.51 Å, normal distance of 3.40 Å and interaction energy of −2.73 kcal/mol, calculated at the accurate CCSD(T)/CBS level of theory [18]. This structure is only slightly less stable than the global minimum for the benzene dimer, which has T-shaped geometry with C-H/π interactions and an interaction energy of −2.84 kcal/mol [18].

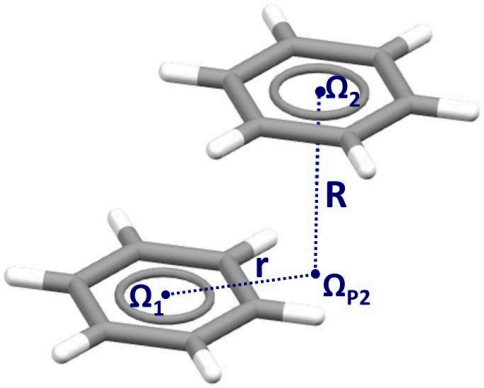

Figure 1. Geometrical parameters that describe stacking interactions between benzene molecules. Ω_1 and Ω_2 are centers of interacting rings, and Ω_{P2} is the projection of the center Ω_2 onto the plane of the other benzene. Normal distance **R** is the distance between Ω_2 and Ω_{P2}, while horizontal displacement (offset) **r** is the distance between Ω_1 and Ω_{P2}.

Theoretical calculations have, however, shown that aromaticity is not a defining feature of stacking interactions [21] and that stacking interactions can be made stronger if one or both aromatic constituents are replaced with nonaromatic ones [22]. Interestingly, first examples of stacking interactions, which include nonaromatic molecules, were given prior to these calculations by analyzing the crystal structures deposited in the Cambridge Structural Database [2]. These interactions were formed between the aromatic and chelate ring of square planar transition metal complexes [23]. Chelate rings are highly stable cyclic systems, which are formed when a metal simultaneously binds to two atoms of a bidentate ligand. Later, it was shown that strong stacking interactions can also be formed between two chelate rings [3].

2.1. Chelate–Aryl Stacking Interactions

Stacking interaction between an organic aromatic ring and a chelate ring of a transition metal complex was first observed in the crystal structure of bis(acetone-1-naphthoylhydrazinato)copper(II) (Figure 2) [23]. This interaction is characterized by the normal distance of R = 3.49 Å and horizontal displacement of r = 1.46 Å, which is very similar to classical parallel-displaced aryl–aryl stacking interaction.

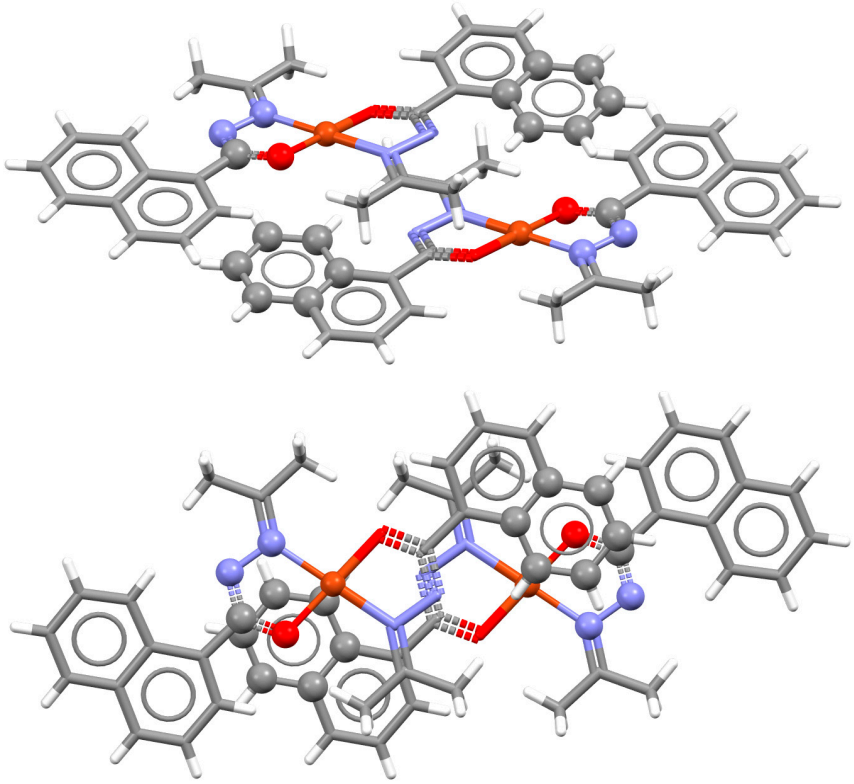

Figure 2. Two views of the intermolecular chelate–aryl stacking interactions with r = 1.46 Å and R = 3.49 Å in the crystal structure of bis(acetone-1-naphthoylhydrazinato)copper(II) (CSD refcode MABNUZ) [23]. Interacting chelate and aromatic rings are presented in ball-and-stick style, while other atoms are presented in capped stick style. Atom colors: carbon—dark gray, hydrogen—white, oxygen—red, nitrogen—blue, copper—light brown.

At approximately the same time, the first intramolecular stacking interaction between the aromatic and chelate ring was observed in the crystal structure of square pyramidal aqua-(1,10-phenanthroline)-(2-benzylmalonato)-copper(II) (Figure 3) [24]. This "aryl–metal chelate ring π–π interaction" [24] was discussed as the new structural evidence of the metalloaromaticity of the copper(II)-(aromatic α,α′-diimine) chelate ring. It was later shown that many chelate rings do not satisfy the magnetic criteria for aromaticity [25].

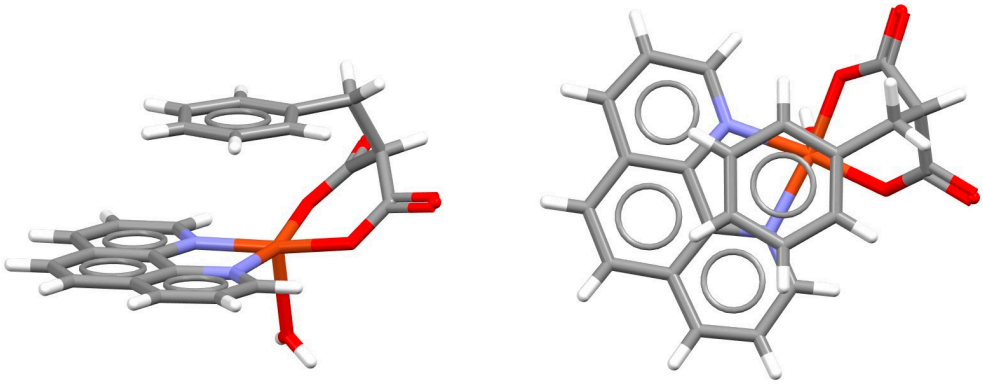

Figure 3. Two views of the intramolecular chelate–aryl stacking interaction with r = 0.92 Å and R = 3.36 Å in the crystal structure of aqua-(1,10-phenanthroline)-(2-benzylmalonato)-copper(II) (CSD refcode VACSUO) [24]. Atom colors: carbon—dark gray, hydrogen—white, oxygen—red, nitrogen—blue, copper—light brown.

The early examples of chelate–aryl stacking interactions prompted an analysis of crystal structures that contain square planar copper(II) complexes and C_6 aromatic rings. This study revealed that the distances between copper atoms and carbon atoms of aromatic rings are shorter if the copper atom is part of a chelate ring [26]. A systematic study of crystal structures containing C_6 aromatic rings and square planar complexes of all transition metals showed that the presence of chelate rings influences the mutual orientation of the aromatic ring and transition-metal complex, as well as the metal–carbon distances [27]. Namely, there is a tendency toward small interplanar angles if the transition metal complex contains a chelate ring (Figure 4a), meaning that rings are parallel [27]. Also, for many transition metal complexes that contain chelate rings, the shortest metal–carbon distance is smaller than the sum of van der Waals radii of metal and carbon atoms (Figure 4b). If the transition metal complex does not contain a chelate ring, the aromatic ring prefers to be orthogonal to the mean plane of the complex, and the metal–carbon distances tend to be larger than in the case of complexes with chelate rings (Figure 4). These parameters are considered the structural evidence for the formation of stacking interaction between chelate and aromatic rings [27]. Interestingly, all of the studied chelate rings have delocalization of π-electrons, which, together with their ability to form stacking interactions, raises further speculations regarding their aromaticity [25]. The composition of five-membered chelate rings forming stacking interactions with C_6 aromatic rings in crystal structures is dominantly MNCCN (M denotes metal), while six-membered chelate rings forming chelate–aryl stacking are usually MNCCCO rings; metals are mostly Ni, Pd, Cu and Pt [22].

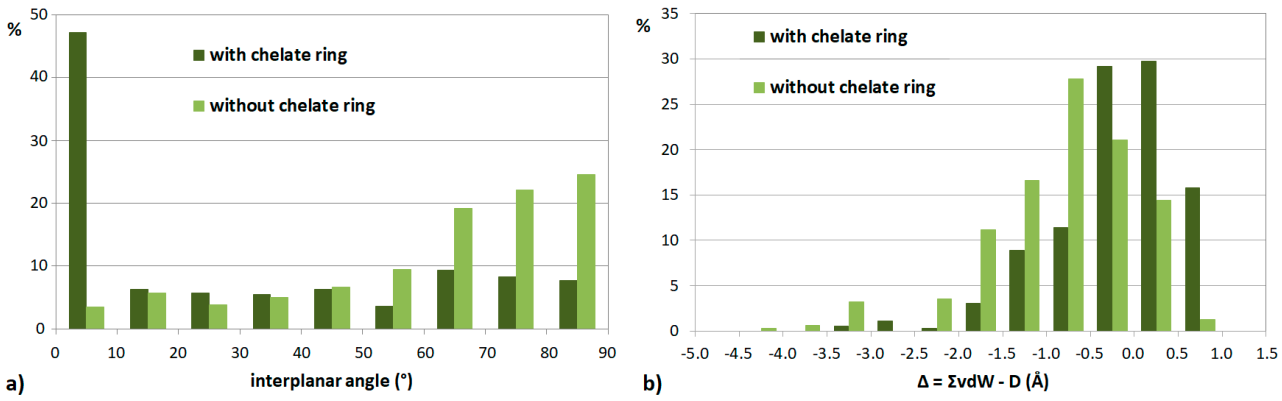

Figure 4. Distribution of interplanar angle (**a**) and the difference between the sum of van der Waals radii and the shortest metal–carbon distance D (**b**) in CSD crystal structures that contain aromatic rings and transition metal complexes with square planar geometry.

The study of chelate–aryl interactions in the CSD crystal structures also showed that when the square planar transition metal complex and aromatic ring are approximately parallel, the displacement angle β is predominantly between 15° and 35° (Figure 5). This shows that the typical arrangement of chelate–aryl stacking interaction is parallel-displaced [27], which is similar to classical aryl–aryl stacking interactions. The detailed study of stacking interactions between the aromatic ring and chelate rings of typical metals (Ni, Pd, Pt, Cu) showed that the arrangements in chelate–aryl stacking interactions are very similar regardless of the metal [28].

Aside from square planar and square pyramidal complexes, chelate–aryl stacking can be formed in octahedral complexes. An interesting example is a hexacoordinated ruthenium complex, which contains terpyridine, bipyridine and imidazole ligands, where intramolecular chelate–aryl stacking interaction is formed (Figure 6). Namely, an imidazole ligand contains phenyl substituents, and it is rotated so that chelate–aryl stacking of the phenyl substituent and chelate ring of the terpyridine ligand is enabled (Figure 6) [29].

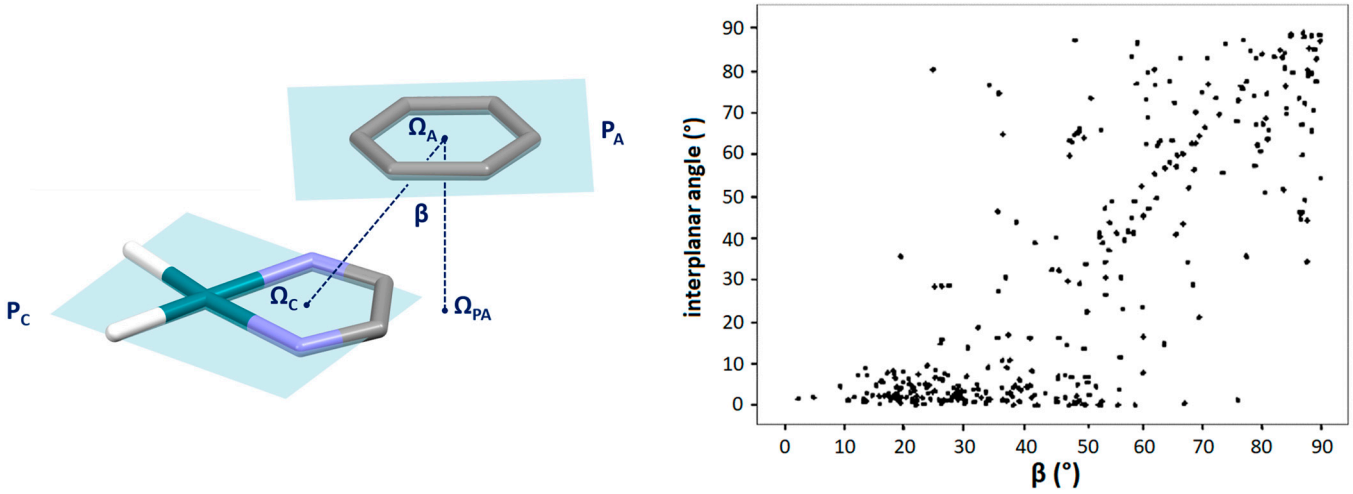

Figure 5. The correlation of the displacement angle β with the angle between the mean planes of chelate and aromatic rings (interplanar angle). The displacement angle β is the angle defined by the line connecting the centers of chelate and aromatic rings (Ω_C and Ω_A, respectively) and the normal of the aromatic ring center onto the chelate ring plane, which is defined by the line connecting the aromatic ring center (Ω_A) and its projection onto the chelate ring plane (Ω_{PA}). Interplanar angle is the angle formed between the chelate ring plane (P_C) and aromatic ring plane (P_A), which are colored light blue.

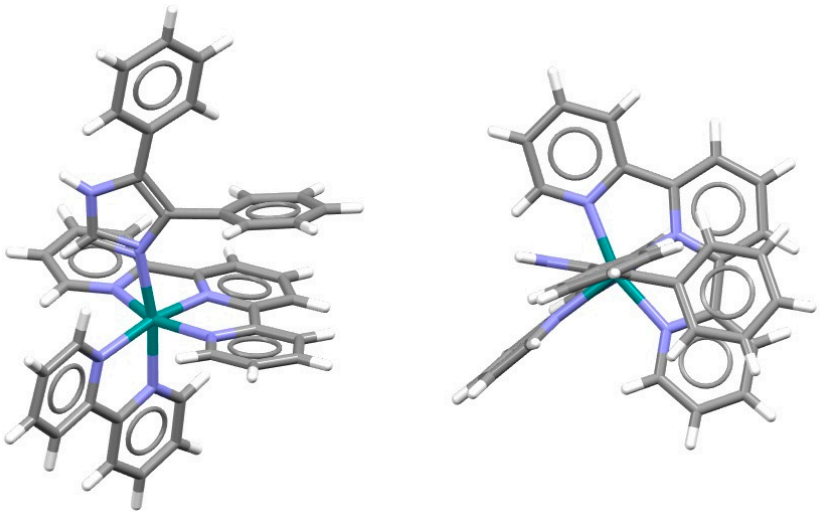

Figure 6. Intramolecular chelate–aryl stacking interaction (r = 1.55 Å and R = 3.32 Å) in the crystal structure of (2,2′-bipyridine)-(4,5-diphenylimidazole)-(2,2′:6′,2′-terpyridine)-ruthenium(II) bis(hexafluorophosphate) methanol solvate (CSD refcode FEPXII) [29]. Atom colors: carbon—dark gray, hydrogen—white, nitrogen—blue, ruthenium—green.

Intramolecular chelate–aryl stacking can be encountered in the crystal structures of coordination polymers. Folded conformation of the copper complex with bipyridine and tryptophane is favored by intramonomer chelate–aryl stacking interaction between the bipyridine chelate ring and C_6 aromatic ring of a tryptophanato ligand, as well as intermonomer π–π stacking between bipyridine ligands (Figure 7). Similar interactions can be observed if bipyridine is replaced with phenanthroline [30].

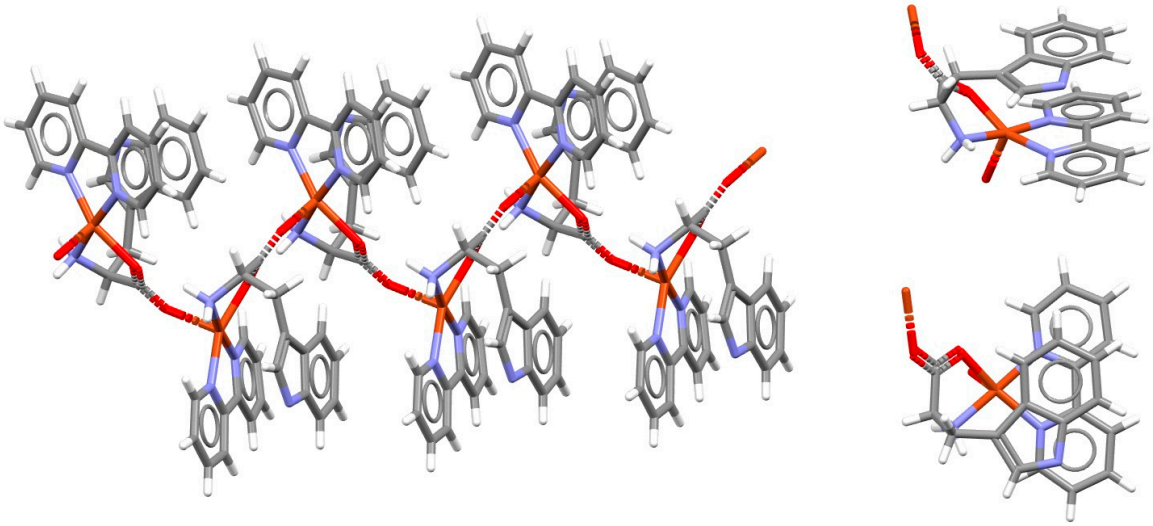

Figure 7. Intramolecular chelate–aryl stacking interactions in the crystal structure of polymeric catena-((PP)-(μ2-L-tryptophanato)-(2,2′-bipyridyl)-copper(II) perchlorate (CSD refcode KIRKIF01) [30], with two views of chelate–aryl stacking in the monomer unit. Atom colors: carbon—dark gray, hydrogen—white, nitrogen—blue, oxygen—red, copper—light brown.

In the crystal structure of a distorted square pyramidal complex of copper with bipyridine and an iminodiacetate derivative containing a nitrophenyl group, intramolecular chelate–aryl stacking cannot be formed due to a large distance between nitrophenyl and coordinated nitrogen. Instead, intermolecular chelate–aryl stacking interaction between the bipyridine ligand of one complex and the nitrophenyl unit of the other complex is formed (Figure 8) [31].

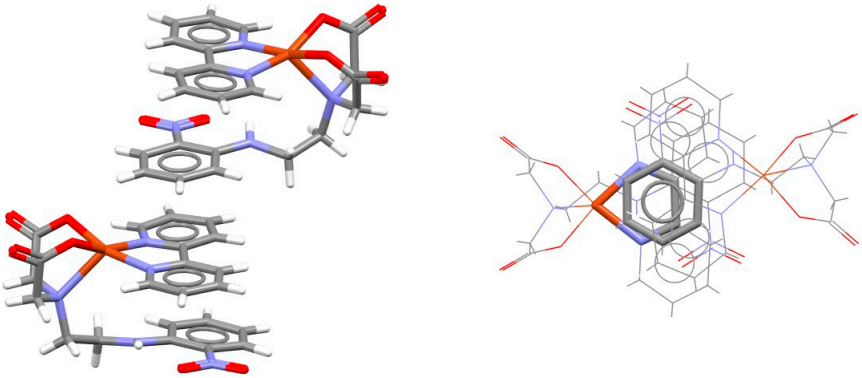

Figure 8. Intermolecular chelate–aryl stacking interaction (r = 0.64 Å and R = 3.35 Å) in the crystal structure of (2,2′-bipyridine-N,N′)-(*fac*-2,2′-((2-((2-nitrophenyl)amino)ethyl)imino)diacetato-N,O,O′)-copper(II) dihydrate (CSD refcode QOZCAK) [31]. Chelate–aryl stacking is highlighted on the right in capped stick style, with the rest of the atoms in wireframe style. Atom colors: carbon—dark gray, hydrogen—white, oxygen—red, nitrogen—blue, copper—light brown.

Intermolecular chelate–aryl stacking can be noted in the crystal structure of a square planar nickel complex containing a chelate ring fused with an aromatic ring and another chelate ring (Figure 9). The aromatic ring of one molecule forms stacking interaction with the sulfur-containing chelate ring of the other molecule (Figure 9) [32]. The preference for the sulfur-containing chelate ring might be due to enhanced dispersion effects.

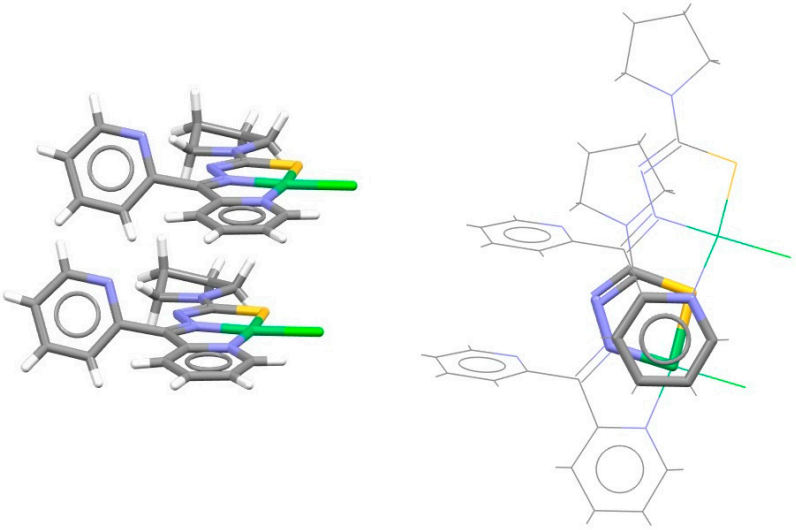

Figure 9. Intermolecular chelate–aryl stacking interaction (r = 0.94 Å and R = 3.49 Å) in the crystal structure of chloro-(di-2-pyridylketone-N4,N4-(butane-1,4-diyl)thiosemicarbazonato)-nickel(II) (CSD refcode AYADAF) [32]. Chelate–aryl stacking is highlighted on the right in capped stick style, with the rest of the atoms in wireframe style. Atom colors: carbon—dark gray, hydrogen—white, sulfur—yellow, nitrogen—blue, chlorine—light green, nickel—green.

It can be noted in previous examples that chelate rings are often fused with aromatic rings. Crystallographic study of stacking interactions of the systems where a chelate ring is fused with an aromatic ring gave insight into the relative strengths of chelate–aryl and aryl–aryl stacking interactions. It was determined that in the majority of these contacts, chelate–aryl distance (d_{CA}) is shorter than aryl–aryl distance (d_{AA}; Figure 10), which indicates that an aromatic ring prefers to stack with a chelate ring, rather than to stack with another aromatic ring [33]. This implied that chelate–aryl stacking interactions are stronger than aryl–aryl stacking interactions.

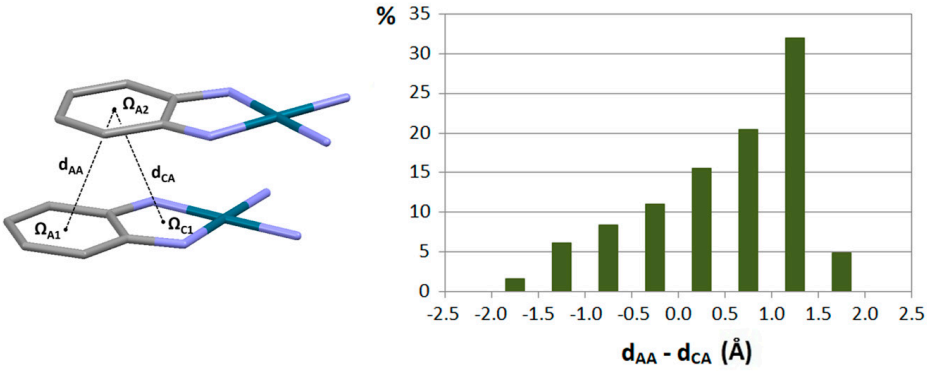

Figure 10. Distribution of the difference in the distances between the centers of aromatic rings (d_{AA}) and between the centers of aromatic and chelate ring (d_{CA}) in the stacking interactions between transition metal complexes with fused chelate and aromatic rings.

The strength of chelate–aryl stacking interactions was the subject of a series of computational studies [34–39]. CCSD(T)/CBS calculations with the extrapolation method of Mackie and DiLabio using the aug-cc-pVTZ and aug-cc-pVQZ basis sets [40], as well as calculations using various DFT methods, were performed on a series of square planar transition metal complexes with *acac*-type chelate rings (*acac* = acetylacetonato). The calculations have shown that the strongest chelate–aryl stacking interactions have parallel-displaced arrangements, with benzene as a model of the aryl ring being located either above the C2 atom or above the metal atom of the chelate ring (Figure 11) [34,36,38]. For the arrangement

with benzene above the C2 atom of the chelate ring, interaction energies are very similar for all complexes, with values around −5.0 kcal/mol (Table 1). However, if benzene is located above the metal atom of the chelate ring, interaction energies vary, depending on the metal in question. The strongest chelate–aryl stacking was calculated for *acac*-type chelate of zinc, with an interaction energy of −7.56 kcal/mol (Table 1) [38]. Considering that benzene–benzene stacking has the interaction energy of −2.73 kcal/mol [18], it can be concluded that chelate–aryl stacking interactions can be significantly stronger than aryl–aryl stacking interactions, which explains their abundance in the CSD crystal structures.

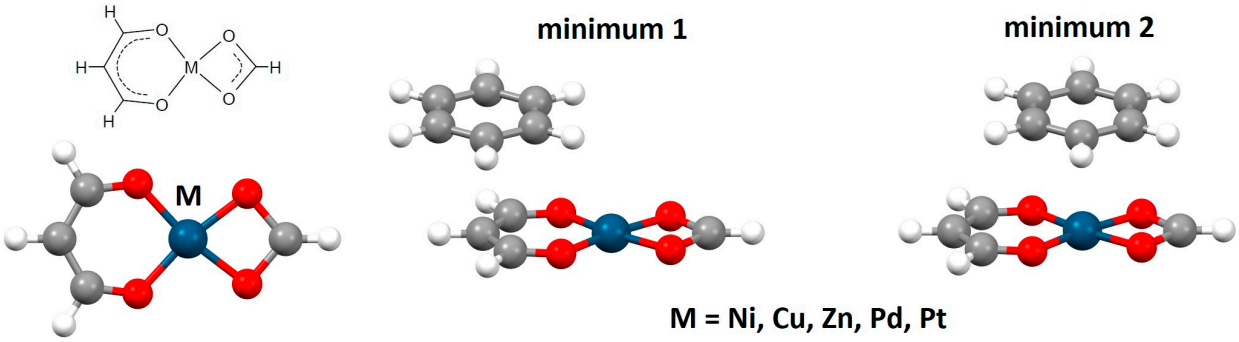

Figure 11. Model systems for calculations of chelate–aryl stacking interactions are made of benzene and square planar complexes of various metals with formate and enolate of malondialdehyde as *acac*-type ligand (*acac* = acetylacetonato). Two minima are found on the potential energy curves for *acac*-benzene chelate–aryl stacking.

Table 1. Geometrical parameters (offset r and normal distance R, both in Å) and interaction energies (ΔE, in kcal/mol) for stacking interactions between benzene and *acac*-type chelate ring in [M(*formate*)(*acac*-type)] complexes. For M = Ni, Cu, Zn, the energies were calculated at ωB97X-D/def2-TZVP level of theory, while for M = Pd, Pt, the energies were calculated at M06-D3/def2-TZVP level of theory. The structures of the dimers are given in Figure 11.

Metal	Minimum 1			Minimum 2		
	r	R	ΔE	r	R	ΔE
Ni [38]	1.3	3.40	−4.82	1.4	3.37	−5.52
Cu [38]	1.2	3.40	−4.92	1.3	3.31	−6.43
Zn [38]	1.0	3.43	−4.93	1.3	3.27	−7.56
Pd [38]	1.2	3.40	−5.15	1.2	3.50	−5.73
Pt [36]	1.2	3.40	−5.36	1.2	3.50	−5.27

In order to gain insight into the nature of chelate–aryl stacking interactions, interaction energies were subjected to decomposition based on Symmetry Adapted Perturbation Theory (SAPT) [41]. The decomposition was performed using the basic SAPT0 level of theory, since it is the only one that is applicable for open-shell systems [42,43], and is therefore the only one that can be used for copper-containing chelate rings. It was shown that dispersion is the most pronounced energy component in chelate–aryl stacking interactions, with significant contribution of electrostatics [38]. The sum of dispersion and exchange components, regarded as net dispersion [44], is very small for chelate–benzene stacking (Table 2), which was also shown to be the case for benzene–benzene stacking (Table 2) [38,44]. Interestingly, when comparing the energy components of stacking interactions of chelates of different metals, it can be noted that the increase in total interaction energy is in good agreement with the increase in the electrostatic energy component (Table 2) [38]. Moreover, the differences in interaction energies of chelate–benzene [38] and benzene–benzene stacking [44,45] correspond to differences in electrostatic energy components (Table 2). Observations similar to those for stacking interactions of *acac*-type chelate rings were also noted for dithiolene chelate complexes [37].

Table 2. Geometrical parameters (offset r and normal distance R, both in Å) and total SAPT0/def2-TZVP interaction energy (ΔE) and its components (ELST—electrostatic, EXCH—exchange, IND—induction, DISP—dispersion, all in kcal/mol) of the most stable stacking interactions between benzene and *acac*-type chelate rings in [M(*formate*)(*acac*-type)] complexes (dimer minimum 2; Figure 11). Net dispersion (NET DISP, in kcal/mol) is the sum of dispersion and exchange components. The decomposition of SAPT2+3/def2-TZVPPD energy of benzene–benzene stacking interaction [45] is given for comparison.

System	r	R	ΔE	ELST	EXCH	IND	DISP	NET DISP
Ni(acac)-benzene	1.4	3.37	−5.97	−4.07	+7.91	−0.80	−9.00	−1.09
Cu(acac)-benzene	1.3	3.31	−6.80	−5.38	+9.53	−1.16	−9.78	−0.25
Zn(acac)-benzene	1.3	3.27	−7.59	−6.38	+10.52	−1.61	−10.12	+0.40
benzene–benzene	1.5	3.50	−2.83	−1.50	+6.58	−0.70	−7.21	−0.62

The arrangements in the dimers with strongest interactions and the pronounced electrostatic component of chelate–aryl stacking can be rationalized with electrostatic potential surfaces of the studied complexes containing chelate rings. The surfaces show positive electrostatic potential above metals (Figure 12), making them good sites for overlapping with negative electrostatic potentials above the benzene ring center (Figure 12) [38]. Moreover, the magnitude of positive potentials increases from Ni to Zn (Figure 12), which produces the same trends in electrostatic energy components and total interaction energies for their chelate–benzene stacking interactions (Table 2) [38].

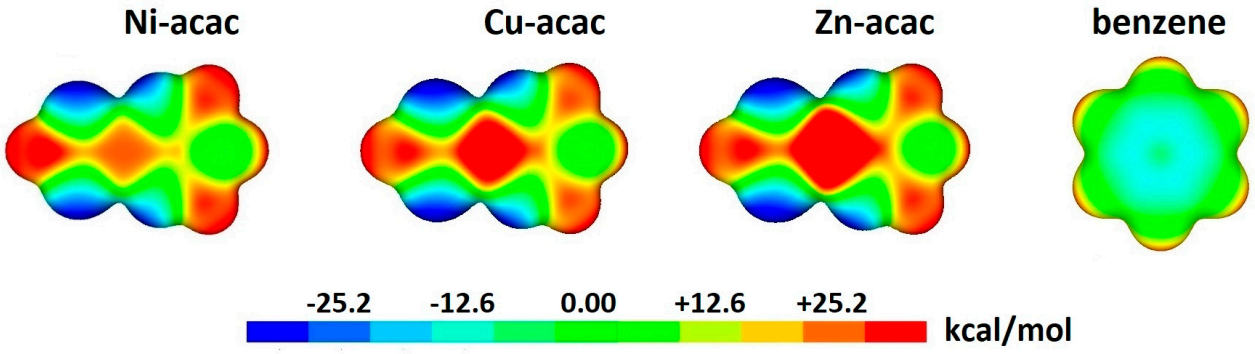

Figure 12. Electrostatic potentials for chelate-containing complexes and benzene plotted at the surface defined by electron density of 0.004 a.u. The potentials were calculated at ωB97X-D/def2-TVZP level of theory.

2.2. Chelate–Chelate Stacking Interactions

The discovery that chelate–aryl stacking interactions are very frequent in the CSD crystal structures has led to assuming that two chelate rings can also form stacking interactions. A detailed CSD survey was conducted according to the criteria given by Janiak, who studied stacking between aromatic rings in transition metal complexes [46]. Namely, two chelate rings are considered forming stacking interaction if the angle between their mean planes is less than 10°, the distance between their centers is shorter than 4.6 Å and their displacement angle β is less than 35° (Figure 13). Since chelate rings are very often fused to organic aromatic rings, interactions of isolated and interactions of fused chelate rings were analyzed separately. The study found 89 chelate–chelate stacking interactions between isolated chelate rings and 1777 chelate–chelate stacking interactions between fused chelate rings [47]. The isolated five-membered chelate rings forming chelate–chelate stacking interactions are mostly of MNCCN composition (M is Ni, Pt or Pd), while six-membered rings mostly have CuOCCCO and CuNCCCO composition [47].

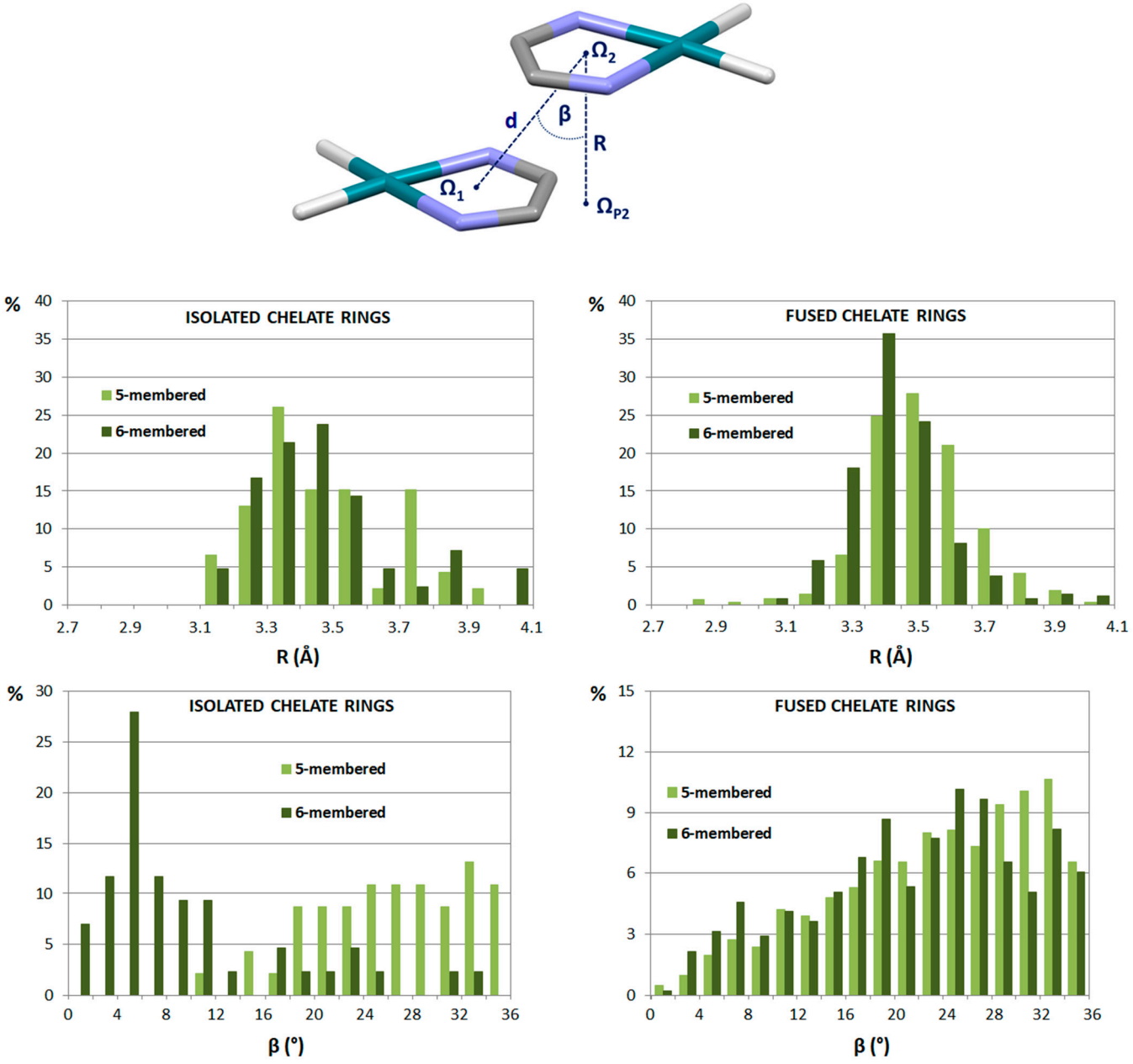

Figure 13. Parameters describing chelate–chelate stacking interactions are distance d between the ring centers (d < 4.6 Å), displacement angle β (β < 35°) and normal distance R. Distributions of normal distance and displacement angle are given separately for stacking interactions of isolated chelate rings and chelate rings fused with aromatic rings. Chelate rings are usually 5-membered and 6-membered.

The majority of chelate–chelate stacking interactions, both of isolated and fused chelate rings, have normal distances between 3.3 Å and 3.5 Å, while displacement angle β values are typically in the range 16–36° (Figure 13), which indicates parallel-displaced arrangement [47]. These geometrical features make chelate–chelate stacking similar to both aryl–aryl and chelate–aryl stacking interactions [3]. The only exception is chelate–chelate stacking interactions of six-membered isolated chelate rings, which have small values of β angles (Figure 13), indicating face-to-face arrangement. Visual inspection has shown that these rings are mostly substituted with bulky groups, which then tend to avoid clashing with each other, giving face-to-face chelate–chelate stacking arrangement [47]. This type

of chelate–chelate stacking can be found in the crystal structure of bis(acetylacetonato)-copper(II) (Figure 14) [48].

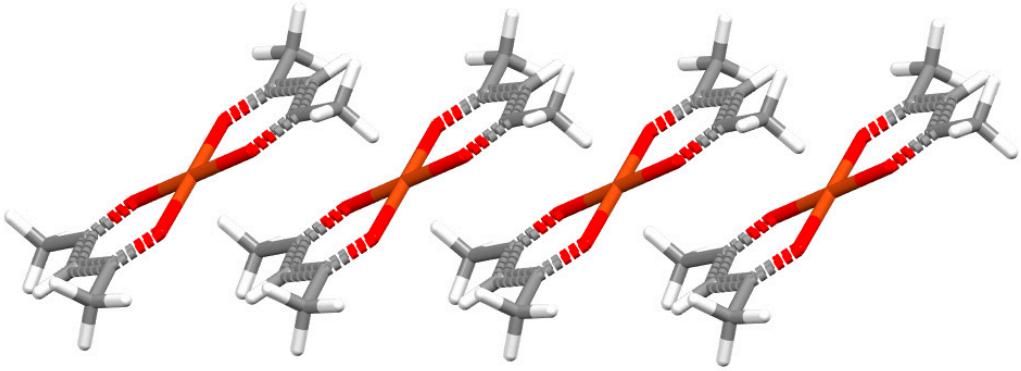

Figure 14. Face-to-face chelate–chelate stacking interaction (r = 0.00 Å, R = 3.15 Å) in the crystal structure of bis(acetylacetonato)copper(II) (CSD refcode ACACCU61) [48]. Atom colors: carbon—dark gray, hydrogen—white, oxygen—red, copper—light brown.

Three typical orientations of stacked chelate rings can be singled out, based on the values of torsion angle τ defined by metals and ring centers (Figure 15). The most abundant are chelate–chelate stacking interactions with antiparallel orientation. One of the many examples of this orientation of stacked chelate rings is encountered in the crystal structure of a palladium complex with an ethyl-2-hydroxy-4-styryl-4-oxo-2-butenoate ligand [49], where six-membered isolated chelate rings of *acac*-type stack in parallel-displaced arrangement (Figure 16). From this crystal structure, it is implied that chelate–chelate stacking is stronger than aryl–aryl stacking, since the formation of chelate–chelate stacking interaction prevents larger overlap of phenyl rings (Figure 16).

For complexes with fused rings, chelate–chelate stacking is often combined with chelate–aryl stacking. The structure of a nickel complex with aromatic hydrazone contains a system of three fused rings (two chelate and one aromatic), which form an antiparallel stacking arrangement with central chelate–chelate stacking interaction surrounded by two chelate–aryl stacking interactions (Figure 17) [50].

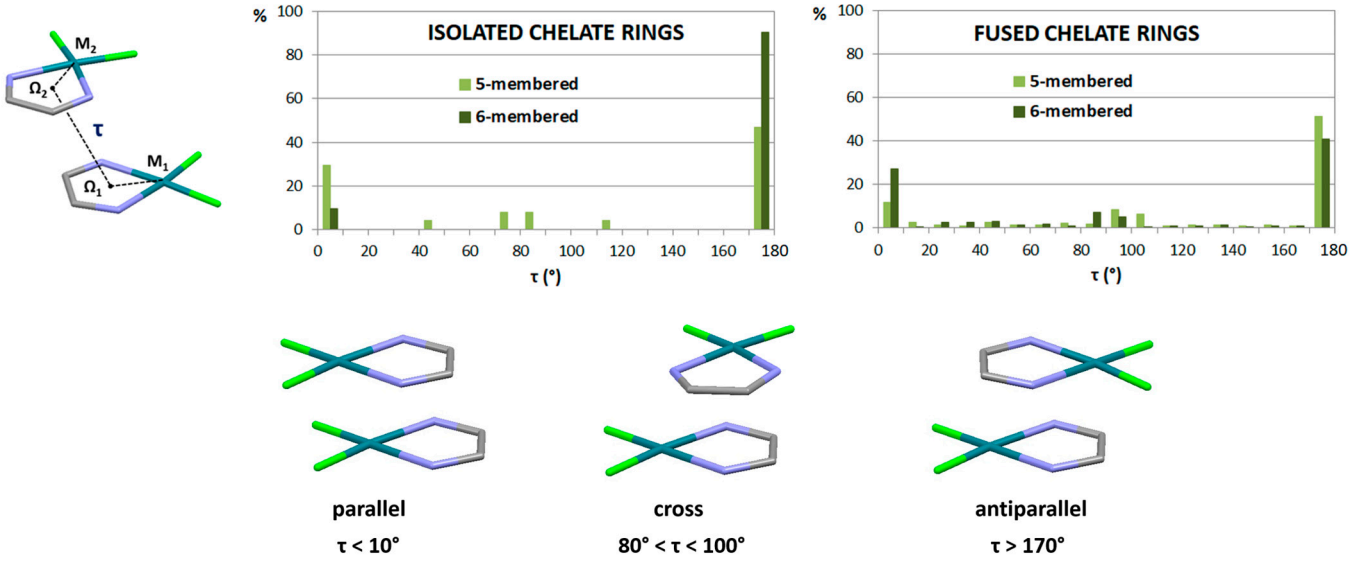

Figure 15. Distributions of torsion angle τ (M_1-Ω_1-Ω_2-M_2) for chelate–chelate interactions found in the CSD crystal structures. Three typical orientations of chelate rings obtained with this analysis are parallel, cross and antiparallel orientation.

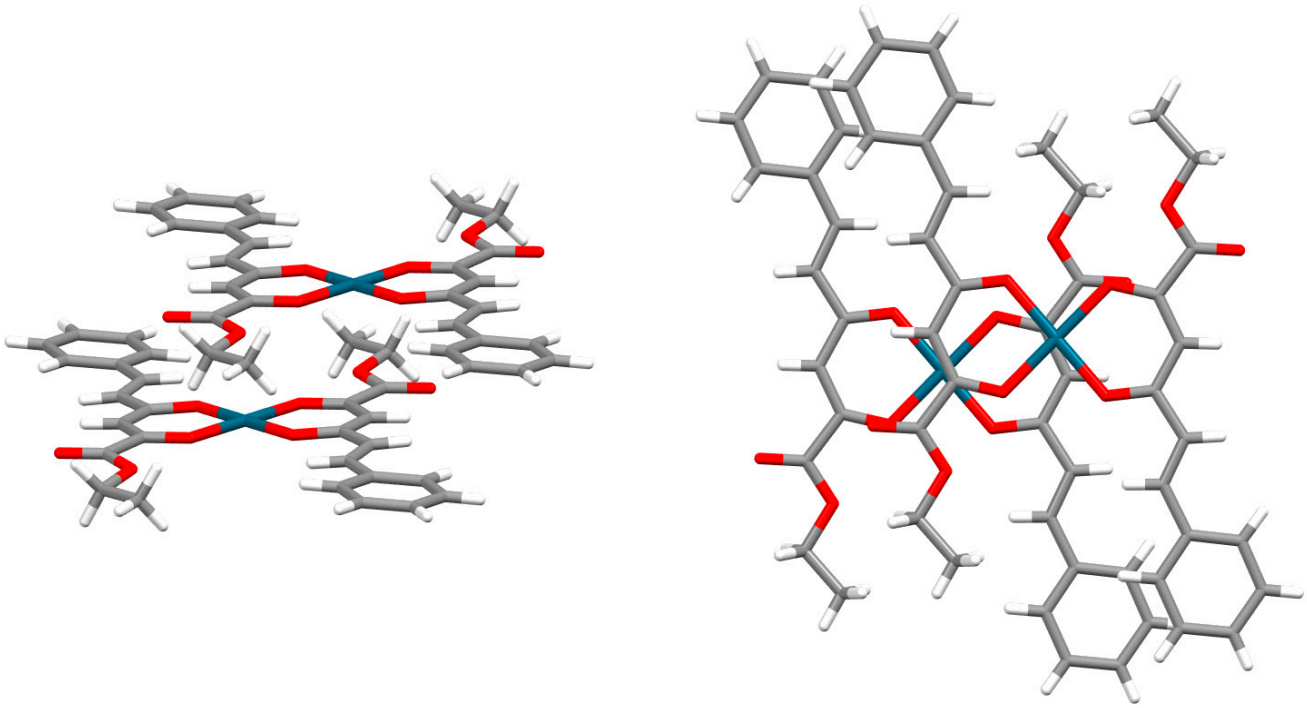

Figure 16. Parallel-displaced chelate–chelate stacking interaction in antiparallel orientation (r = 1.32 Å, R = 3.29 Å) in the crystal structure of palladium complex with ethyl-2-hydroxy-4-styryl-4-oxo-2-butenoate ligand [49]. Atom colors: carbon—dark gray, hydrogen—white, oxygen—red, palladium—blue.

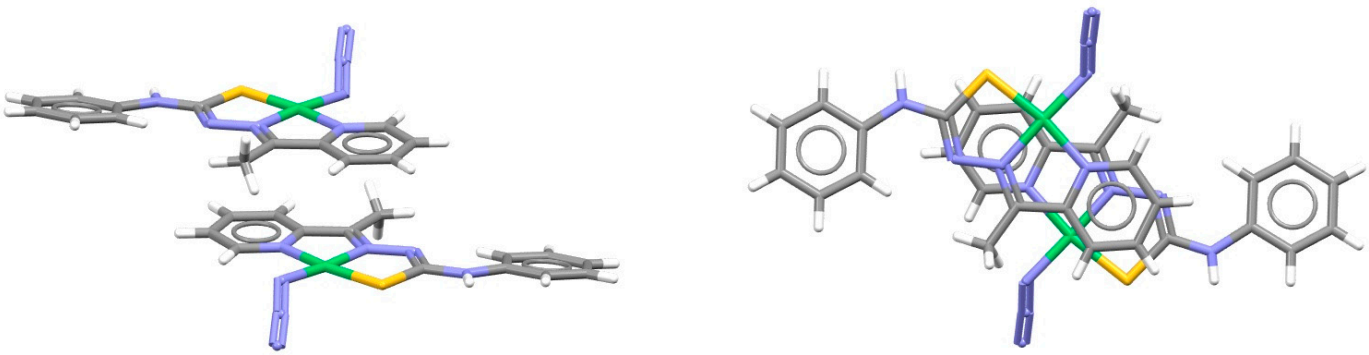

Figure 17. Chelate–chelate stacking interaction (r = 1.05 Å and R = 3.42 Å) combined with two chelate–aryl stacking interactions in the crystal structure of azido-(N-phenyl-N′-(1-(pyridin-2-yl)ethylidene)carbamohydrazonothioato)-nickel(II) (CSD refcode XAMVOZ) [50]. Atom colors: carbon—dark gray, hydrogen—white, nitrogen—blue, sulfur—yellow, nickel—green.

Parallel orientation is less encountered than the antiparallel one in CSD crystal structures (Figure 15) [47]. It can usually be encountered when a square planar complex contains two identical chelate rings, which enables them to overlap almost entirely by forming two simultaneous chelate–chelate stacking interactions. Such parallel orientation was found, among others, in the crystal structure of bis(2-(1H-pyrazol-5-yl)pyridinato)platinum(II) (Figure 18), where two N,N-type chelate rings fused with aromatic rings form a pair of chelate–chelate stacking interactions [51].

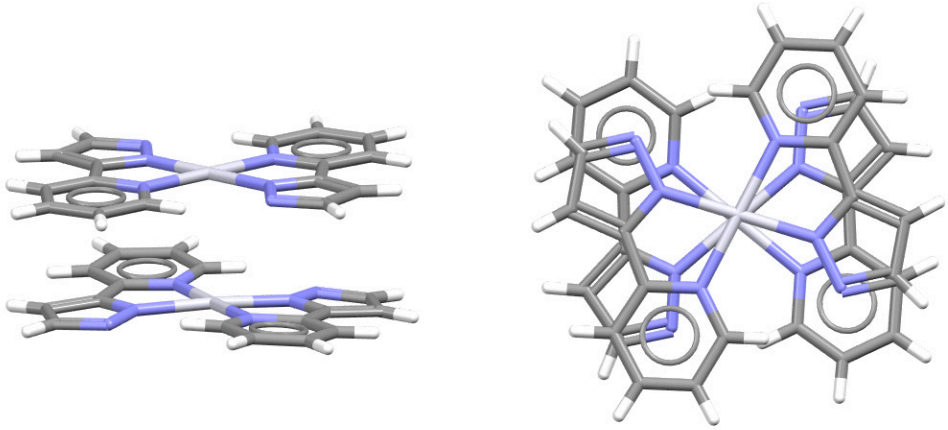

Figure 18. Parallel-displaced chelate–chelate stacking interactions with parallel orientation of fused chelate rings (r = 0.71 Å, R = 3.32 Å) in the crystal structure of bis(2-(1H-pyrazol-5-yl)pyridinato)platinum(II) (CSD refcode USIRUK) [51]. Atom colors: carbon—dark gray, hydrogen—white, nitrogen—blue, platinum—light gray.

An interesting example of parallel orientation is encountered in the crystal structure of a biimidazole complex of rhodium (Figure 19). The molecules of this complex form three geometrically different and alternating chelate–chelate stacking interactions, all of which are parallel-displaced and in parallel orientation of the complexes (Figure 19). Very similar stacking interactions are found in crystal structures of this cationic complex with several different counteranions [52].

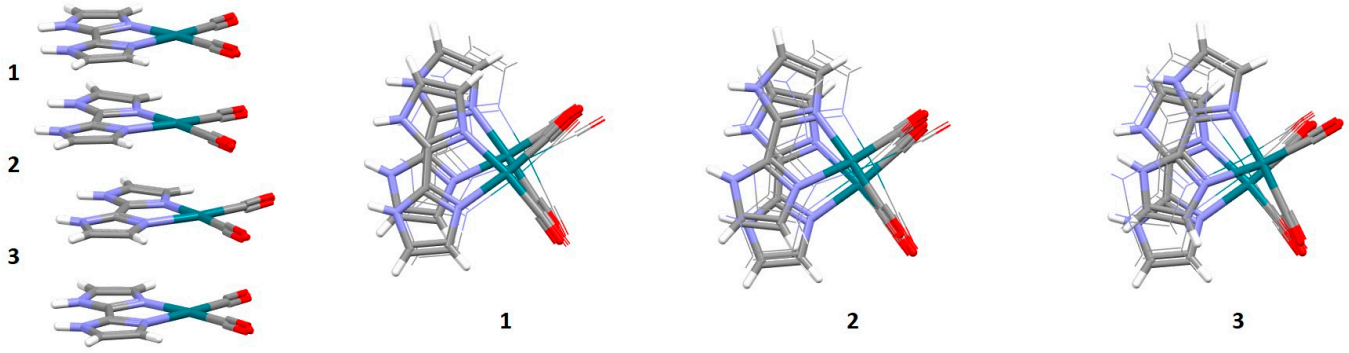

Figure 19. Three different chelate–chelate stacking interactions in crystal structure of hexakis(Dicarbonyl-(2,2′-bi-imidazole)-rhodium(I) dicarbonyl-dichloro-rhodium(I) pentachloride dichloromethane solvate tetrahydrate (CSD refcode RUXPUW) [52]. All individual interactions are parallel-displaced (**1** r = 1.10 Å and R = 3.31 Å, **2** r = 0.86 Å and R = 3.39 Å, **3** r = 1.26 Å and R = 3.29 Å). Molecules forming individual interactions are highlighted in capped stick style, while the other atoms are in wireframe style. Atom colors: carbon—dark gray, hydrogen—white, nitrogen—blue, oxygen—red, rhodium—dark green.

The analysis of crystal structures containing cross orientation of chelate–chelate stacking showed that this orientation is characteristic for fused chelate rings, where it is always encountered together with parallel or (more often) antiparallel orientation [47]. In the crystal structure of a copper complex containing fused five-membered and six-membered rings, there is the antiparallel chelate–chelate stacking interaction of six-membered chelate rings, and two simultaneous cross chelate–chelate stacking interactions between the six-membered and five-membered ring (Figure 20) [53].

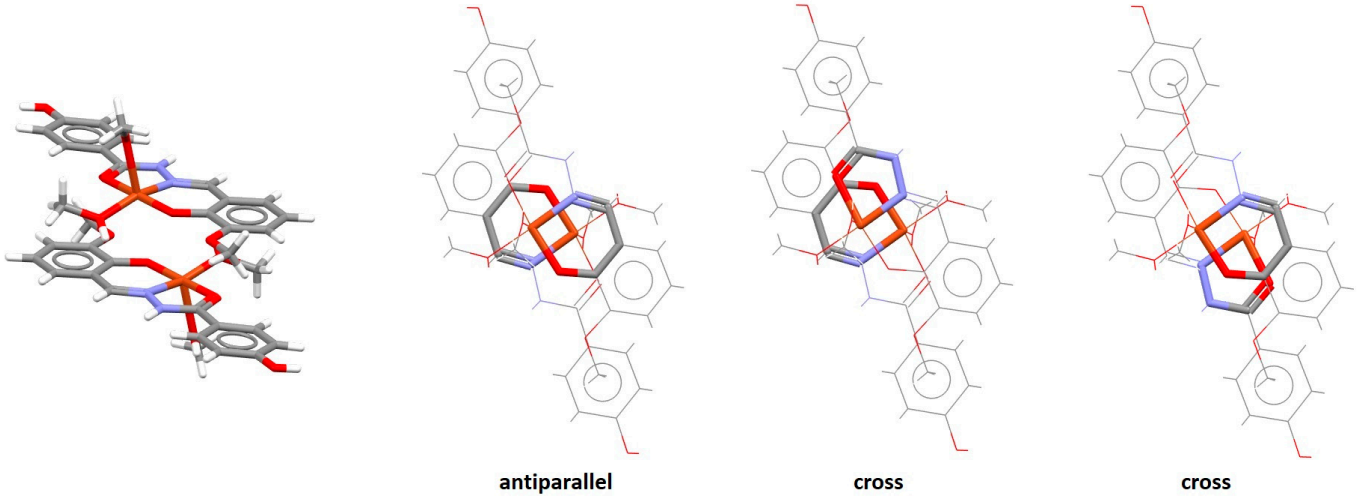

Figure 20. Simultaneous antiparallel (r = 1.83 Å and R = 3.40 Å) and cross chelate–chelate stacking interactions (r = 1.41 Å and R = 3.36 Å) in the crystal structure of (4-hydroxy-N′-(2-oxy-3-methoxybenzylidene)benzohydrazide)-bis(methanol)-copper(II) nitrate methanol solvate (CSD refcode XETXEB) [53]. The antiparallel and cross orientations are highlighted in capped stick style, while the other atoms are in wireframe style. Atom colors: carbon—dark gray, hydrogen—white, nitrogen—blue, oxygen—red, copper—light brown.

Quantum chemical calculations on *acac*-type chelates (Figure 21) have shown that chelate–chelate stacking interactions are strongest in antiparallel orientation [54], which can explain the dominance of this orientation in crystal structures (the other reasons may include the existence of the center of symmetry in antiparallel orientation) [47]. As in the case of chelate–aryl stacking interactions, interaction energies can greatly vary depending on the metal. It can be noted that *acac*-type chelates of Ni, Pd and Pt stack with similar interaction energies of about −9.5 kcal/mol (Table 3) [54], while Cu and Zn chelates form significantly stronger antiparallel chelate–chelate stacking interactions (−11.70 kcal/mol and −14.58 kcal/mol; Table 3) [38]. On the other hand, the strongest parallel chelate–chelate stacking surpasses only the interaction energy of −6.28 kcal/mol [54]. The strength of chelate–chelate stacking interactions in antiparallel orientation increases going from Ni to Zn chelates, in accordance with the increase in the electrostatic component of interaction energy (Table 4) [38]. This is owed to double overlapping of positive electrostatic potentials above metals and negative electrostatic potentials above C2 atoms of chelate rings (Figures 12 and 21). Hence, strong antiparallel orientations are a consequence of favorable electrostatic interactions.

Interestingly, interaction energies in cross orientation are very similar to those in parallel orientation (Table 3). Still, parallel orientation is more often encountered in crystal structures than cross orientation (Figure 15) [47], probably due to the existence of elements of symmetry in parallel orientation.

From the interaction energies, it can be concluded that chelate–chelate stacking interactions are stronger than chelate–aryl and aryl–aryl stacking interactions [3]. Chelate–chelate stacking owes its strength to a very pronounced electrostatic energy component, which in some cases even exceeds the dispersion energy (Table 4), which is typically the dominant one for stacking interactions of aromatic molecules [38]. Similar energies and nature of interactions are observed for stacking interactions between dithiolene chelate rings [37,38]. Overall, crystallographic and computational data imply that stacking interactions of chelate rings are very important noncovalent interactions that must be considered when observing and discussing the packing of molecules in the crystal structures and other systems.

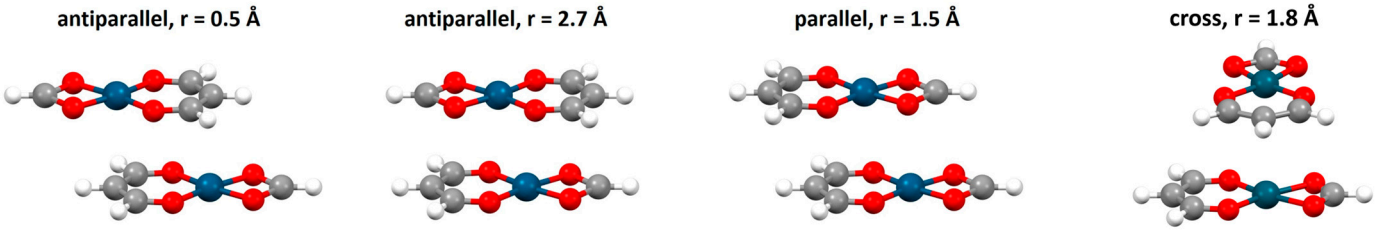

Figure 21. Minima on potential energy curves for stacking interactions between *acac*-type chelate rings of various metals (Ni, Cu, Zn, Pd, Pt).

Table 3. Geometrical parameters (offset r and normal distance R, both in Å) and interaction energies (ΔE, in kcal/mol) for stacking interactions between two *acac*-type chelate rings in [M(*formate*)(*acac*-type)] complexes. For all the metals, the energies were calculated at LC-ωPBE-D3BJ/aug-cc-pVDZ level of theory. The structures of the dimers are given in Figure 21.

Metal	Antiparallel			Parallel			Cross		
	r	R	ΔE	r	R	ΔE	r	R	ΔE
Ni [38]	0.5	3.13	−9.47	1.8	3.20	−4.80	1.8	3.25	−4.98
Cu [38]	0.4	3.01	−11.70						
Zn [38]	0.4	2.88	−14.58						
Pd [54]	2.7	3.30	−9.30	1.8	3.20	−5.97	1.8	3.30	−5.56
Pt [54]	2.7	3.30	−9.73	1.5	3.30	−6.28	1.8	3.40	−6.13

Table 4. Geometrical parameters (offset r and normal distance R, both in Å) and total SAPT0/def2-TZVP interaction energy (ΔE) and its components (ELST—electrostatic, EXCH—exchange, IND—induction, DISP—dispersion, all in kcal/mol) of the most stable stacking interactions between two *acac*-type chelate rings in [M(*formate*)(*acac*-type)] complexes (antiparallel orientation; Figure 21). Net dispersion (NET DISP, in kcal/mol) is the sum of dispersion and exchange components.

Metal	r	R	ΔE	ELST	EXCH	IND	DISP	NET DISP
Ni	0.5	3.13	−10.11	−11.99	+15.60	−1.82	−11.89	+3.71
Cu	0.4	3.01	−12.54	−16.67	+21.42	−3.47	−13.82	+7.60
Zn	0.4	2.88	−15.39	−23.21	+30.67	−6.67	−16.18	+14.49

3. Stacking Interactions of Hydrogen-Bridged Rings

Hydrogen-bridged rings are the rings in which one of the bonds is an intramolecular hydrogen bond. These rings may have no π-bonds, which makes them single-bond hydrogen-bridged rings (**SBHB**; Figure 22). More known are resonance-assisted hydrogen-bridged rings (**RAHB**), in which hydrogen donor and acceptor atoms are connected by a π-conjugated system (Figure 22). In these rings, there are synergistic effects between the hydrogen bond and resonance, which reinforce H-bond strengthening and π-delocalization [55,56], making them very interesting from theoretical and experimental points of view [57,58]. Interestingly, some theoretical studies show that the reason for the stability of intramolecular hydrogen bonds in RAHB rings is not resonance, but simply the σ-skeleton of the systems, which provides the close proximity of the hydrogen donor and hydrogen acceptor [59,60].

Hydrogen-bridged rings have found an application in numerous areas, ranging from biomolecules to synthesis and materials. The denaturant activity of a guanidinium cation towards proteins with aromatic side chains is owed to the formation of hydrogen-bridged rings [61,62]. The formation of a hydrogen-bridged ring was shown to have a critical role in E/Z isomeric resolution [63,64]. The supramolecular design based on the creation of six-membered intramolecular hydrogen-bonded rings was shown to improve the temperature range of liquid crystals [65]. RAHB rings are also shown to drive the photoluminescence of ethyl N-salicylideneglycinate dyes [58]. Moreover, optical properties of alternating

phenylene–pyridinylene copolymers can be finely tuned due to the formation of RAHB rings [66].

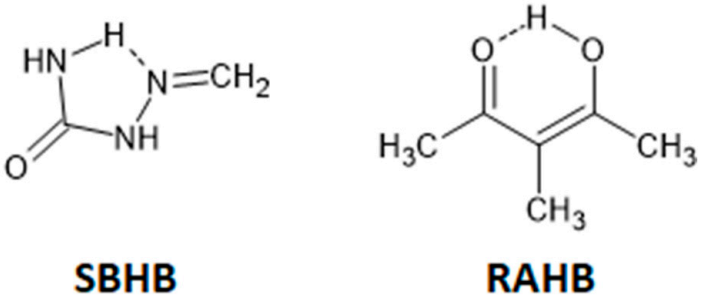

Figure 22. Examples of single-bond hydrogen-bridged (SBHB) and resonance-assisted hydrogen-bridged rings (RAHB).

Similar to chelate rings in transition metal complexes, hydrogen-bridged rings can form stacking interactions, in spite of not being aromatic. These stacking interactions were recognized and their geometrical parameters were described based on the crystal data deposited in the Cambridge Structural Database [7–10,67,68]. Moreover, calculated interaction energies show that the stacking interactions of hydrogen-bridged rings are stronger than stacking interactions of aromatic molecules [7–10,67,68]. For both types of hydrogen-bridged rings (SBHB and RAHB), stacking interactions between two hydrogen-bridged rings were studied, as well as interactions of hydrogen-bridged rings and C6-aromatic rings.

3.1. Stacking Interactions of Single-Bond Hydrogen-Bridged Rings

The search of CSD derived a total of 978 crystal structures with planar hydrogen-bridged rings with all covalent bonds within the ring being single and acyclic and all atoms in the ring being planar (single-bond hydrogen-bridged rings, SBHB; Figure 22) [7]. Interaction between two SBHB rings, as well as between SBHB and a C6-aromatic ring, is characterized by the distance between the centers of the rings that is shorter than 4.5 Å (Figure 23). In this way, a total of 307 SBHB/SBHB and 493 SBHB/aromatic interactions were found [7,8]. For SBHB/SBHB interactions, there is a very high tendency for small interplanar angles (86%), while SBHB/aromatic contacts showed a smaller tendency for interplanar angles below 10° (45%; Figure 24). Therefore, a total of 264 SBHB/SBHB and 221 SBHB/aromatic stacking interactions were found in the CSD crystal structures [7,8].

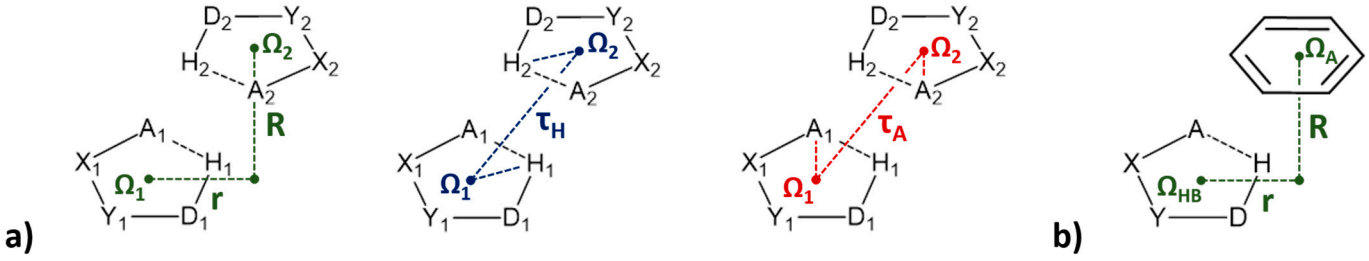

Figure 23. Geometrical parameters used for the description of stacking interactions between two SBHB rings (**a**) and between SBHB and C6-aromatic ring (**b**). Ω denotes the ring centroid; X and Y are any atoms adjacent to hydrogen bond acceptor A and donor D atoms. R and r mark normal distance and offset value, respectively. Additionally, mutual orientations of two SBHB rings are determined with τ_H and τ_A torsion angles.

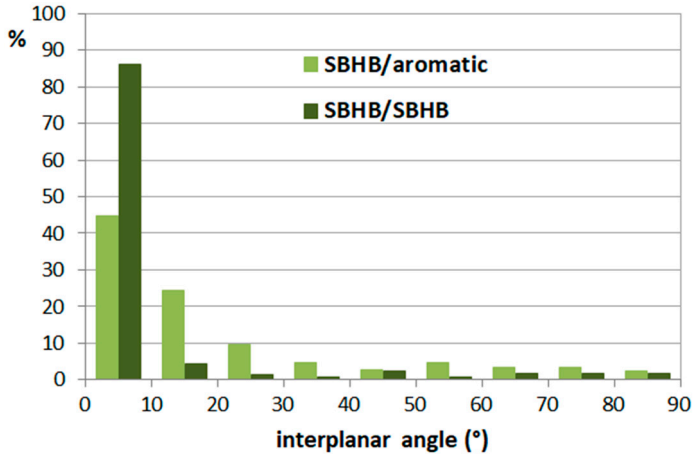

Figure 24. Distribution of interplanar angles for SBHB/SBHB and SBHB/aromatic interactions in the CSD crystal structures.

The analysis of the geometrical parameters shows that most of the stacking interactions of SBHB rings have normal distances in the range between 3.0 Å and 3.5 Å (Figure 25), which makes them very similar to stacking interactions of organic aromatic rings. The horizontal displacement values are mostly between 1.0 Å and 3.0 Å (Figure 25), indicating parallel-displaced arrangement [7,8]. Moreover, in the case of SBHB/SBHB stacking interactions, most of the contacts have both τ_H and τ_A torsion angles at around 180° (Figure 23), showing preferred head-to-tail, or antiparallel orientation [7], similar to that for the stacking of chelate rings [47].

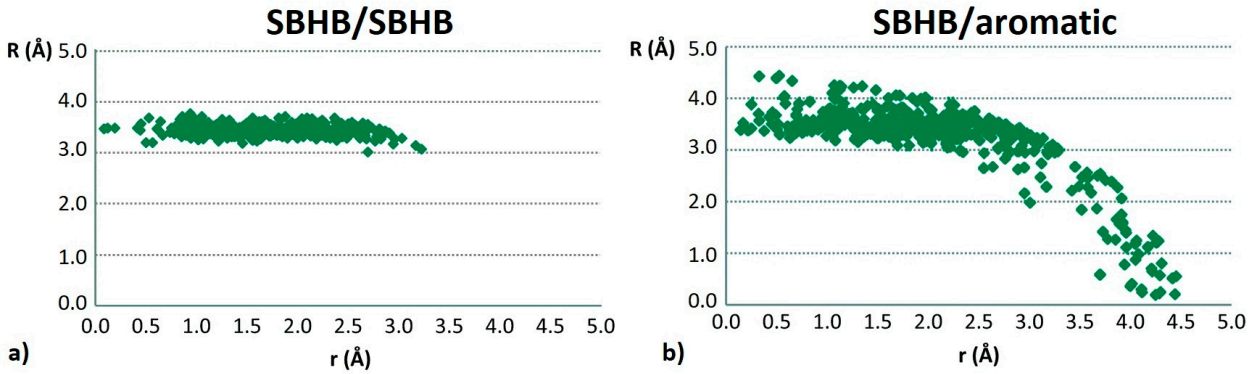

Figure 25. Dependence of normal distance R on the offset values r for stacking interactions between two SBHB rings (**a**) and between SBHB ring and C6-aromatic ring (**b**).

It was determined that 94% of all SBHB/SBHB contacts have HNCNN composition of the hydrogen-bridged ring, out of which 75% have sulfur as a substituent of the C atom [7]. Therefore, stacking interactions between two single-bond hydrogen-bridged rings are mostly encountered in the crystal structures containing derivatives of thiosemicarbazide. One of many examples of this parallel-displaced stacking is found between two thiosemicarbazones coordinated to copper(I) ions (Figure 26) [69].

SBHB rings are also formed in crystal structures of derivatives of semicarbazide, which has oxygen instead of sulfur as a substituent on the C atom. The CSD survey has shown that 20% of all SBHB/SBHB stacking interactions found in the CSD are between HNCNN rings with an oxygen substituent [7]. Therefore, another type of compounds forming SBHB/SBHB stacking interactions is semicarbazides. One example of this stacking interaction is presented in Figure 27 [70].

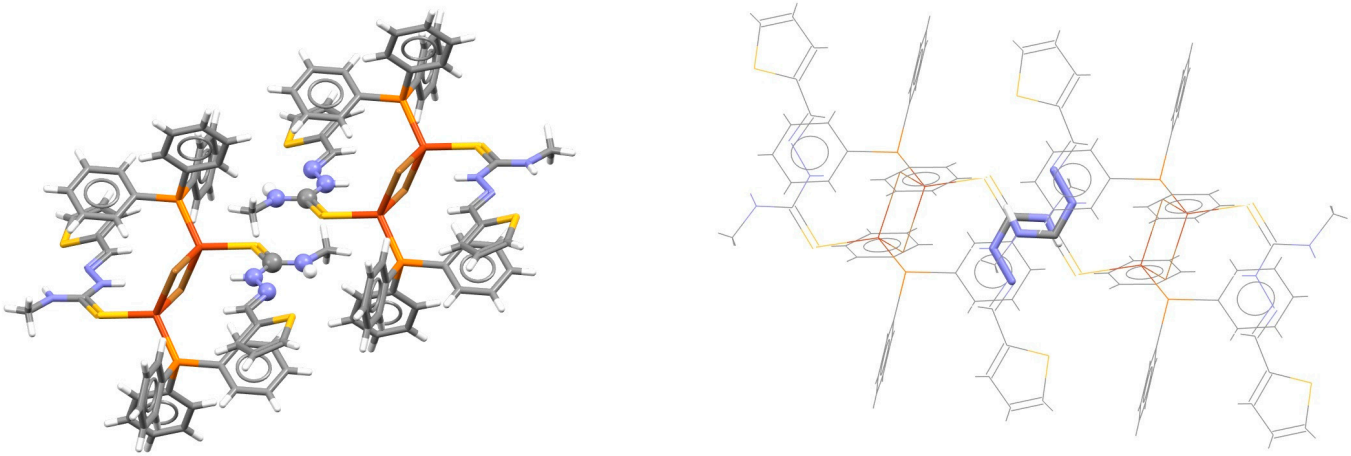

Figure 26. Parallel-displaced stacking interaction (r = 1.59 Å and R = 3.34 Å) between two single-bond hydrogen-bridged rings in the crystal structure of bis(μ^2-bromo)-bis(N-methyl-2-(2-thienylmethylene)hydrazinecarbothioamide)-bis(triphenylphosphine)-di-copper(I) (CSD refcode KUGTAI) [69]. The atoms of SBHB rings forming the stacking interaction are presented in ball-and-stick style on the left and capped stick on the right, while atoms not belonging to the SBHB ring are presented in capped stick style on the left and in wireframe style on the right. Atom colors: carbon—dark gray, hydrogen—white, nitrogen—blue, sulfur—yellow, phosphorus—orange, copper—light brown.

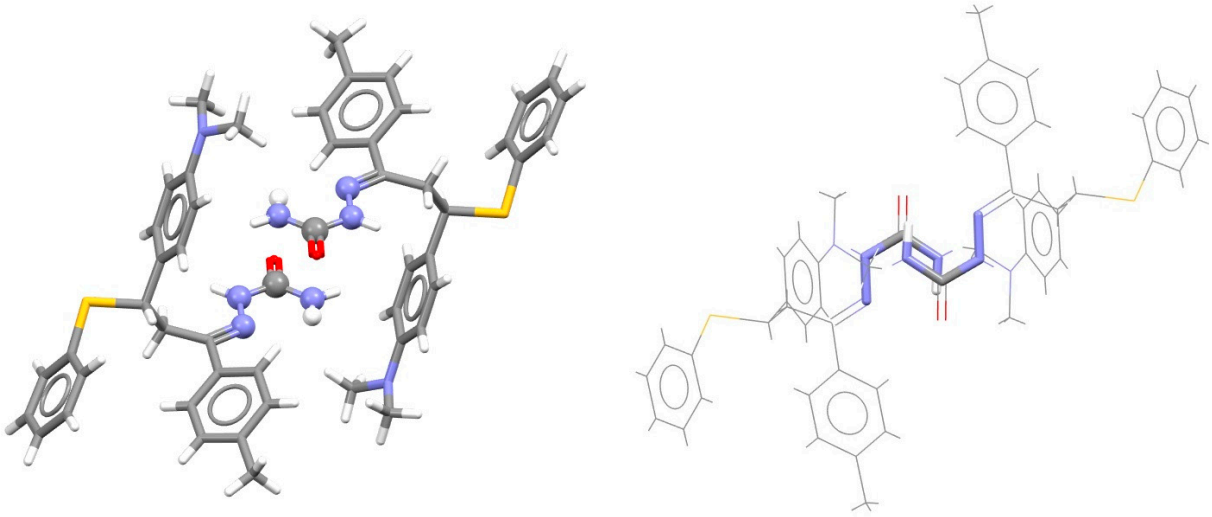

Figure 27. Parallel-displaced stacking interaction (r = 1.64 Å and R = 3.21 Å) between two single-bond hydrogen-bridged rings in the crystal structure of (3-(4-(N,N-dimethylamino)phenyl)-1-(4-methylphenyl)-3-(phenylsulfanyl)propylidene)semicarbazide (CSD refcode OCANAI) [70]. The atoms of SBHB rings forming the stacking interaction are presented in ball-and-stick style on the left and capped stick on the right, while atoms not belonging to the SBHB ring are presented in capped stick style on the left and in wireframe style on the right. Atom colors: carbon—dark gray, hydrogen—white, nitrogen—blue, oxygen—red, sulfur—yellow.

The visual inspection of the SBHB/aromatic stacking interactions indicates that most of the contacts are between molecules that contain both C6-aromatic and hydrogen-bridged rings (Figure 28) [8]. These molecules have the possibility for aromatic/aromatic, SBHB/aromatic and SBHB/SBHB stacking interactions. The most frequent are SBHB/aromatic stacking interactions with head-to-tail orientation of the whole molecules (Figure 28), which were found in 58% of all stacking interactions [8]. In 62% of these contacts, two simulta-

neous SBHB/aromatic stacking interactions are encountered, and they are also usually formed with the derivatives of thiosemicarbazide (Figure 28) [71].

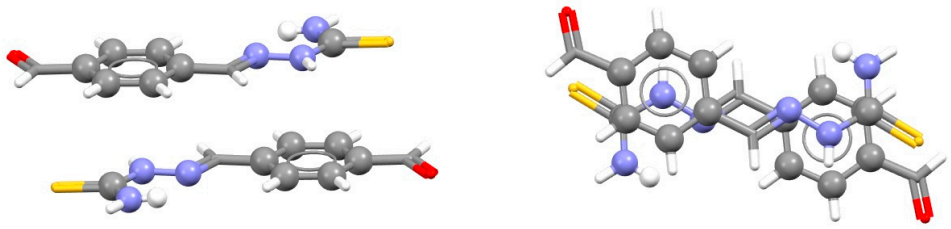

Figure 28. Two simultaneous SBHB/aromatic stacking interactions (r = 0.80 Å and R = 3.38 Å) in the crystal structure of 2-(4-formylbenzylidene)hydrazinecarbothioamide (CSD refcode WOPJES) [71]. Hydrogen-bridged and aromatic rings are presented in ball-and-stick style, while other atoms are given in capped stick style. Atom colors: carbon—dark gray, hydrogen—white, oxygen—red, nitrogen—blue, sulfur—yellow.

An interesting case is the crystal structure containing pyridine-2-carbaldehydethiosemicarbazonium, which has an SBHB ring next to a five-membered resonance-assisted hydrogen-bridged (RAHB) ring and an aromatic ring [72]. Unlike most of the (antiparallel) contacts between such units, these ions are stacked with parallel orientation (Figure 29a), which allows for the formation of simultaneous SHBH/aromatic (Figure 29b), SBHB/RAHB stacking (Figure 29c) and RAHB/aromatic stacking interactions (Figure 29d).

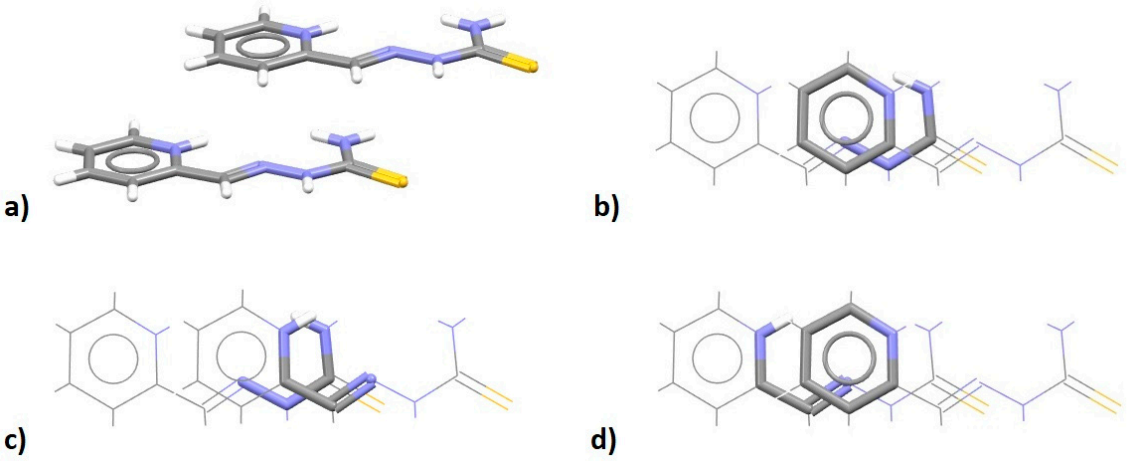

Figure 29. Crystal structure of pyridine-2-carbaldehyde thiosemicarbazonium chloride monohydrate (CSD refcode RAHRAV) [72] contains stacked semicarbazone units (**a**) with SBHB/aromatic (**b**), SBHB/RAHB (**c**) and RAHB/aromatic stacking interactions (**d**). SBHB/aromatic stacking interaction is parallel-displaced (r = 1.46 Å and R = 3.28 Å), as well as the other stacking interactions. Particular interactions are highlighted in capped stick style, with the rest of the atoms in wireframe style. Atom colors: carbon—dark gray, hydrogen—white, nitrogen—blue, sulfur—yellow.

High-level CCSD(T)/CBS calculations of SBHB stacking interaction energies were performed using 2-methylidenehydrazinecarbothioamide as a model molecule, based on the occurrence of this type of hydrogen-bridged rings in the CSD crystal structures [7]. SBHB rings form the strongest stacking interactions in parallel-displaced arrangement, with head-to-tail orientation (Figure 30). The strongest SBHB/SBHB stacking interaction has the energy of −4.89 kcal/mol (Table 5) [7]. On the other hand, the most stable SBHB/benzene stacking interaction is somewhat weaker, with an interaction energy of −4.38 kcal/mol (Table 5) [8]. Nevertheless, both types of stacking interactions of single-bond hydrogen-bridged rings are more stable than stacking interaction between two aromatic (benzene) rings [18]. The SAPT2+3 [73] analysis of SBHB/benzene stacking interaction showed that

the strongest attractive contribution to the total interaction energy is dispersion, which is twice as strong as electrostatics (Table 5) [8]. SBHB/benzene stacking is stronger than benzene/benzene stacking due to more attractive dispersion and (especially) electrostatic energy terms (Table 5) [8].

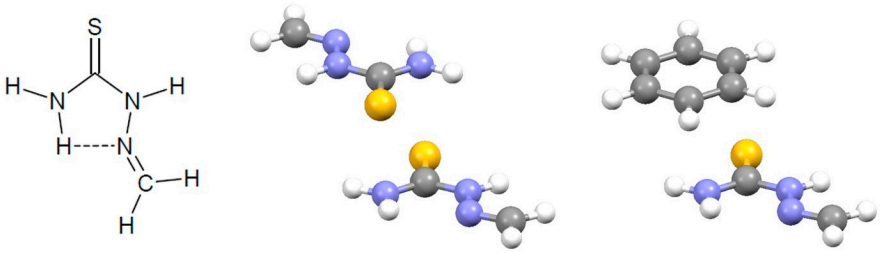

Figure 30. Structure of 2-methylidenehydrazinecarbothioamide, which was selected as the model molecule for single-bond hydrogen-bridged ring, based on the analysis of CSD data. The arrangements of the most stable stacked SBHB/SBHB and SBHB/benzene dimers are presented in ball-and-stick style.

Table 5. Interaction energies (ΔE, in kcal/mol) calculated at the CCSD(T)/CBS level and normal distances (R, in Å) and offset values (r, in Å) for the most stable SBHB/SBHB and SBHB/benzene stacking interactions (Figure 30). The total interaction energy for SBHB/benzene was recalculated at SAPT2+3/aug-cc-pVDZ level of theory (SAPT, in kcal/mol) and decomposed into electrostatic (ELST), exchange (EXCH), induction (IND) and dispersion (DISP) components (all in kcal/mol). The data from SAPT2+3/def2-TZVPPD decomposition of benzene/benzene stacking are given for comparison.

System	r	R	ΔE	SAPT	ELST	EXCH	IND	DISP
SBHB/SBHB [7]	1.0	3.0	−4.89					
SBHB/benzene [8]	1.5	3.2	−4.38	−4.44	−4.29	+9.49	−1.04	−8.59
benzene/benzene [45]	1.5	3.50	−2.79	−2.83	−1.50	+6.58	−0.70	−7.21

SBHB/SBHB stacking interactions can be further stabilized if the SBHB rings contain out-of-plane hydrogen atoms. This gives the possibility for additional simultaneous hydrogen bonds between out-of-plane hydrogen atoms of one ring and electronegative atoms of the other ring [67], as encountered in the crystal structure of hydrazinecarbothioamide (Figure 31) [74]. The large impact of these additional hydrogen bonds was shown with the CCSD(T)/CBS calculations, which showed that the overall interaction in the hydrazinecarbothioamide dimer is twice as strong as the stacking interaction in the 2-methylidenehydrazinecarbothioamide dimer (−9.68 kcal/mol [67] and −4.89 kcal/mol [7], respectively).

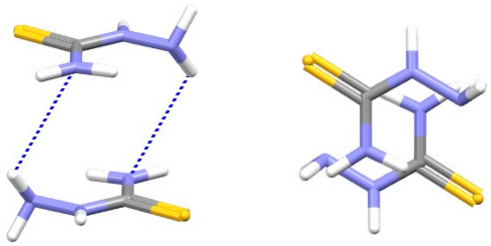

Figure 31. Parallel-displaced SBHB/SBHB stacking interaction (r = 1.02 Å and R = 3.42 Å) with additional hydrogen bonds of out-of-plane hydrogen atoms (N-H···N distance: 3.141 Å) in the crystal structure of hydrazinecarbothioamide (CSD refcode TSCRBZ01) [74]. Atom colors: carbon—dark grey, hydrogen—white, nitrogen—blue, sulfur—yellow.

3.2. Stacking Interactions of Resonance-Assisted Hydrogen-Bridged Rings

In order to study if resonance-assisted hydrogen-bridged rings (RAHB) are capable of forming stacking interactions, the search of crystal structures deposited in the CSD was performed in order to find six-membered RAHB rings with all bonds being acyclic, in order to exclude the presence of rigid fused rings that can also form stacking interactions. This search gave 1543 RAHB rings [9], which was more in comparison to SBHB rings [7]. Using the distance between ring centers shorter than 4.5 Å as the criterion, the search gave a total of 678 interactions between two RAHB rings (Figure 32a), as well as 677 interactions between RAHB and C_6-aromatic rings (Figure 32b). Small interplanar angles (less than 10°) were encountered in 91% of RAHB/RAHB interactions and 59% of RAHB/aromatic interactions. Therefore, a total of 617 RAHB/RAHB stacking interactions [9] and 402 RAHB/aromatic stacking interactions [10] were found in the CSD crystal structures.

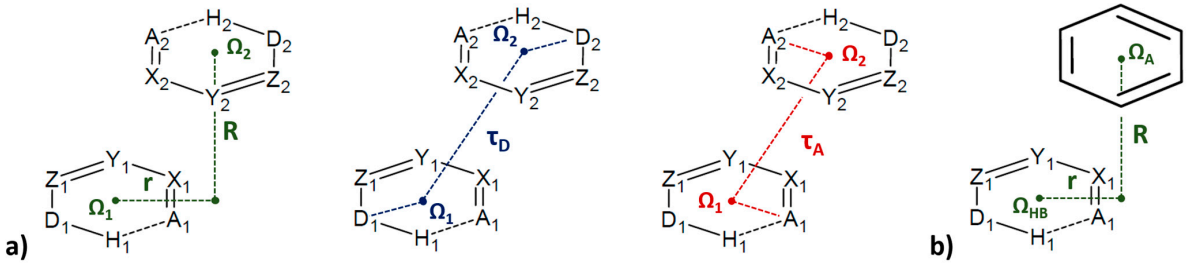

Figure 32. Geometrical parameters used for the description of stacking interactions between two RAHB rings (**a**) and between RAHB and C6-aromatic ring (**b**). Ω denotes the ring centroid; X, Y and Z are any atoms; acceptor and donor atoms (A and D, respectively) include N, O and S atoms. R and r mark normal distance and offset value, respectively. Additionally, mutual orientations of two RAHB rings are determined with τ_D and τ_A torsion angles.

Similar to hydrogen-bridged rings with single bonds (Section 3.1), normal distances in both RAHB/RAHB and RAHB-aromatic stacking are dominantly between 3.0 and 4.0 Å (Figure 33) [9,10], which is also typical for stacking interactions of aromatic organic molecules. These interactions are in most cases parallel-displaced, with horizontal displacements typically in the range 1.0–3.0 Å (Figure 33) [9,10]. The analysis of the mutual orientations of the two interacting RAHB rings showed another similarity with stacking interactions of SBHB rings, and that is the antiparallel orientation of interacting rings [9].

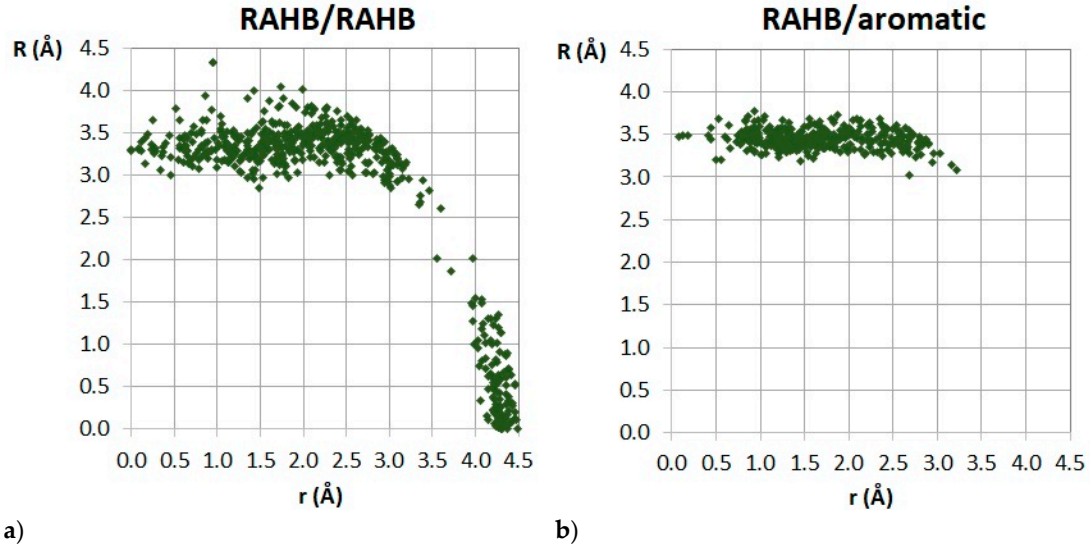

Figure 33. Dependence of normal distance R on the offset values r for stacking interactions between two RAHB rings (**a**) and between RAHB ring and C_6-aromatic ring (**b**).

The compositions of RAHB rings forming most of the stacking interactions are HOCCCO (31%), HNCCCO (28%) and HNNCCO (17%) [9]. The most abundant composition, HOCCCO, usually belongs to β-diketones in enol form or β-hydroxy esters. Parallel-displaced RAHB/RAHB stacking interaction is found in the crystal structure of one such ester (Figure 34) [75]. Since this RAHB ring is connected to an organic aromatic ring, there is a simultaneous aromatic–aromatic stacking interaction, which also has parallel-displaced arrangement (Figure 34).

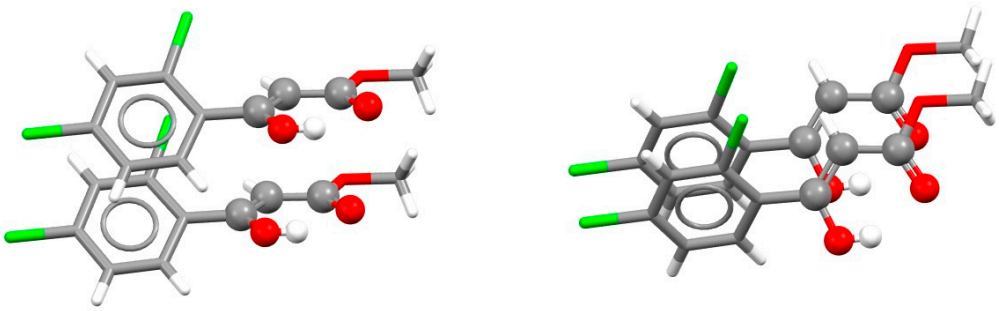

Figure 34. Parallel-displaced stacking interaction between two RAHB rings (r = 1.55 Å and R = 3.50 Å) in the crystal structure of (Z)-methyl-3-(2,4-dichlorophenyl)-3-hydroxyacrylate (CSD refcode SAFNEU) [75]. RAHB ring is shown in ball-and-stick style, while other atoms are shown in capped stick style. Atom colors: carbon—dark gray, hydrogen—white, oxygen—red, chlorine—green.

The RAHB/RAHB stacking between HNCCCO rings was observed in the crystal structure of a Z diastereoisomer of the push–pull alkene containing pyrrolo[2,3-*b*]quinoxaline (Figure 35) [76]. The central π-bond of this alkene is a part of the RAHB ring, which forms a dimer with the neighboring molecule via RAHB/RAHB stacking (Figure 35). Aside from RAHB/RAHB stacking interactions, these dimers are additionally stabilized by aromatic C-H/π interactions, as well as aromatic–aromatic stacking with large horizontal displacement (Figure 35) [76].

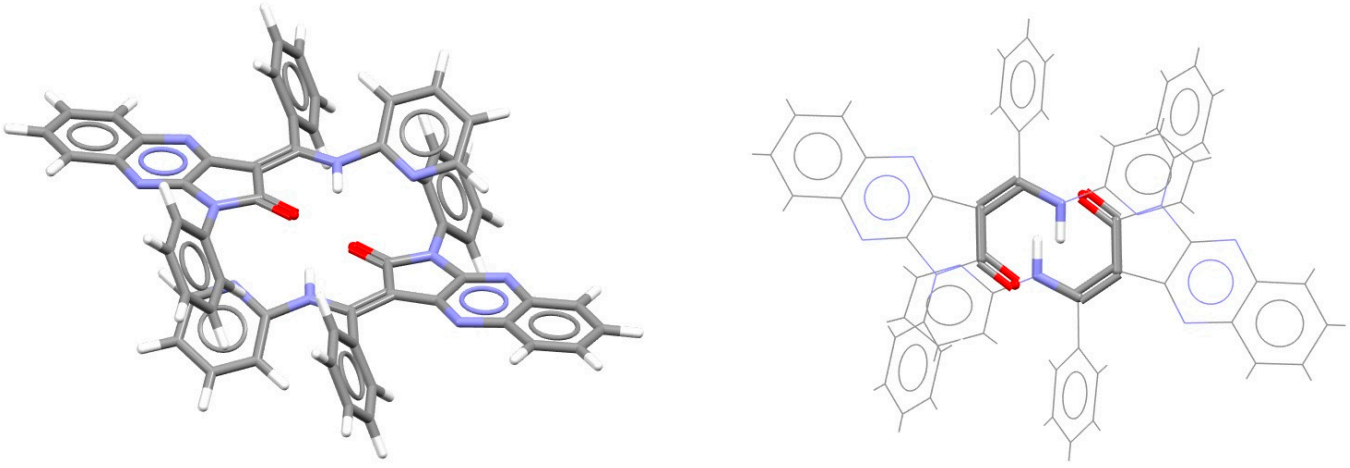

Figure 35. Parallel-displaced RAHB/RAHB stacking interaction (r = 1.75 Å and R = 3.44 Å) in the crystal structure of (Z)-3-[(pyridin-2-ylamino)phenylmethylidene]-1,3-dihydro-2H-1-phenylpyrrolo[2,3-b]quinoxalin-2-one (CSD refcode LUYWAF) [76]. The view on the right has RAHB/RAHB stacking highlighted in capped stick style, with the rest of the atoms in wireframe style. Atom colors: carbon—dark gray, hydrogen—white, oxygen—red, nitrogen—blue.

As in the case of SBHB/aromatic stacking, RAHB/aromatic stacking interactions are often encountered in the structures that contain molecules with both RAHB and aromatic rings (Figure 36). In this way, two simultaneous parallel-displaced RAHB/aromatic stack-

ing interactions can be formed, as it is the case in the crystal structure of the ester with HNNCCO ring composition (Figure 36) [77].

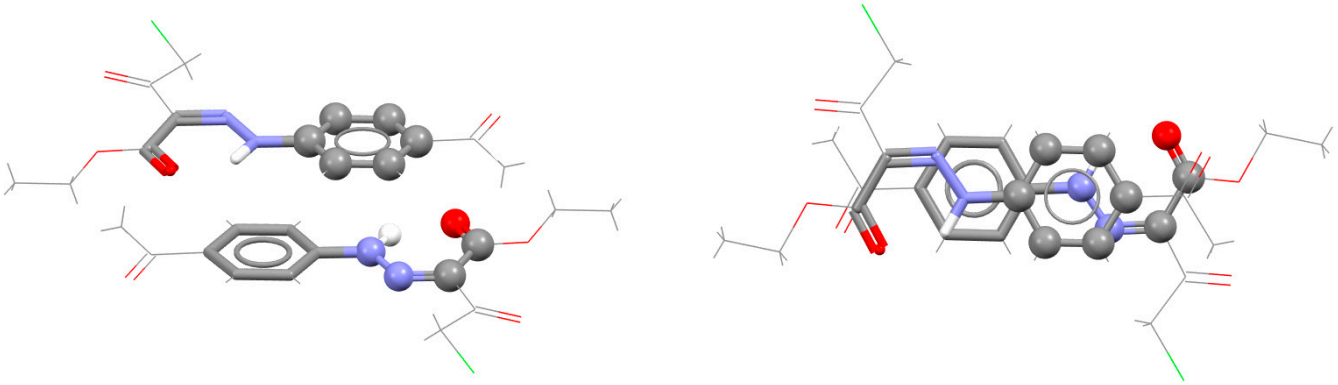

Figure 36. Two simultaneous parallel-displaced RAHB/aromatic stacking interactions (r = 1.55 Å and R = 3.40 Å) in the crystal structure of (Z)-ethyl-2-(2-(4-acetylphenyl)hydrazono)-4-chloro-3-oxobutanoate (CSD refcode PIDGEP) [77]. One RAHB/aromatic contact is shown in capped stick style, and the other one in ball-and-stick style. The remaining atoms are shown in wireframe style. Atom colors: carbon—dark gray, hydrogen—white, oxygen—red, nitrogen—blue, chlorine—green.

If RAHB and the aromatic ring are not coplanar, only one RAHB/aromatic stacking interaction can be formed. In one example, regarding the crystal structure of phenyl-substituted β-diketimine of the *NacNac* type, where the aromatic and RAHB ring cannot be planar due to the presence of methyl groups on RAHB rings, a single RAHB/aromatic stacking interaction is formed between an unusual HNCCCN RAHB ring of one molecule and phenyl ring of the other molecule (Figure 37) [78].

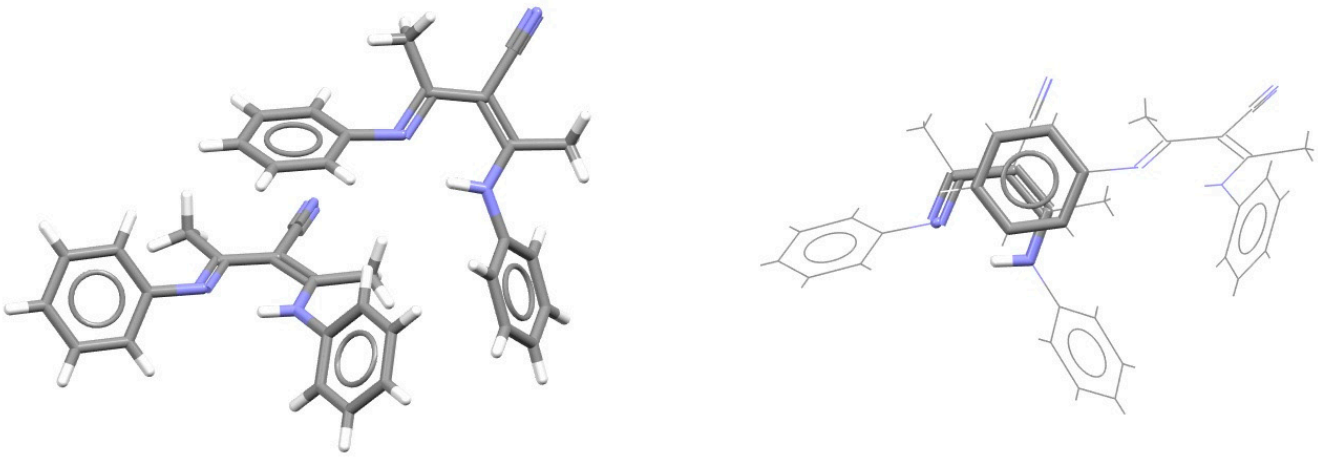

Figure 37. Parallel-displaced RAHB/aromatic stacking interaction (r = 1.55 Å and R = 3.68 Å) in the crystal structure of 3-anilino-2-(N-phenylethanimidoyl)but-2-enenitrile (CSD refcode NAVZAN) [78]. This stacking interaction is highlighted on the right in capped stick style, with the remaining atoms in wireframe style. Atom colors: carbon—dark gray, hydrogen—white, nitrogen—blue.

The model systems for quantum chemical calculations of stacking interaction energies are based on the three most frequent types of RAHB rings in the CSD crystal structures (Figures 38 and 39). The CCSD(T)/CBS interaction energies for both RAHB/RAHB and RAHB/aromatic stacking interactions vary depending on the ring composition (Table 6). In general, RAHB/RAHB stacking is stronger than RAHB/benzene stacking (−4.74 kcal/mol and −3.54 kcal/mol, respectively; Table 6) [9,10]. Comparison with interaction energies of stacking interactions of single-bond hydrogen-bridged rings (Section 3.1) shows that the

strongest interactions for RAHB systems are somewhat weaker than the strongest interactions for SBHB systems (Table 5) [7–10]. However, when compared with the interaction energies between stacked benzene molecules (−2.73 kcal/mol) [18], stacking interactions of RAHB rings are stronger. The calculations have also shown that RAHB stacking interaction energies are significantly preserved even at large horizontal displacements [68].

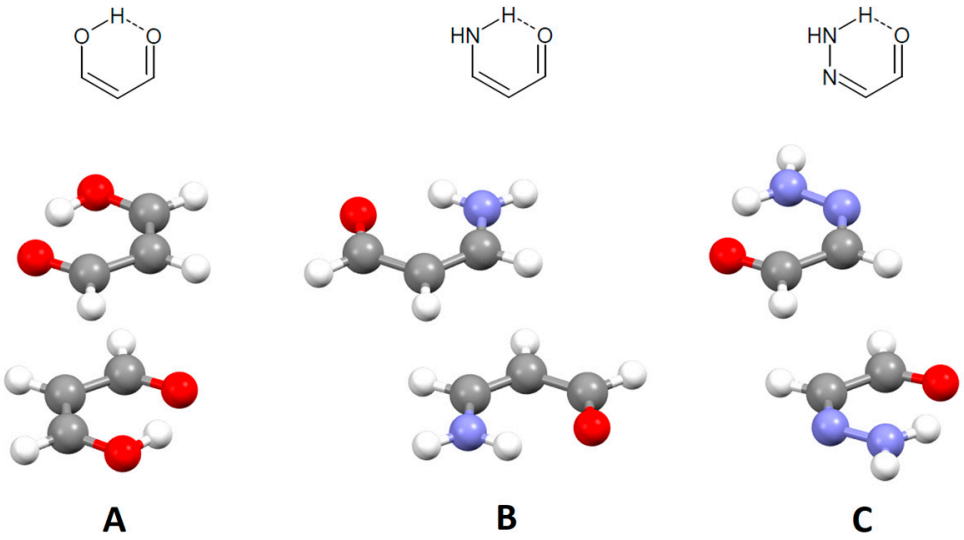

Figure 38. Molecules used for the model systems for quantum chemical calculations of stacking interaction energies between two RAHB rings were (2Z)-3-hydroxyprop-2-enal (**A**), (2Z)-3-aminoprop-2-enal (**B**) and (2Z)-hydrazinylideneacetaldehyde (**C**). Presented are the arrangements with strongest stacking interactions for each system. Atom colors: carbon—dark gray, hydrogen—white, nitrogen—blue, oxygen—red.

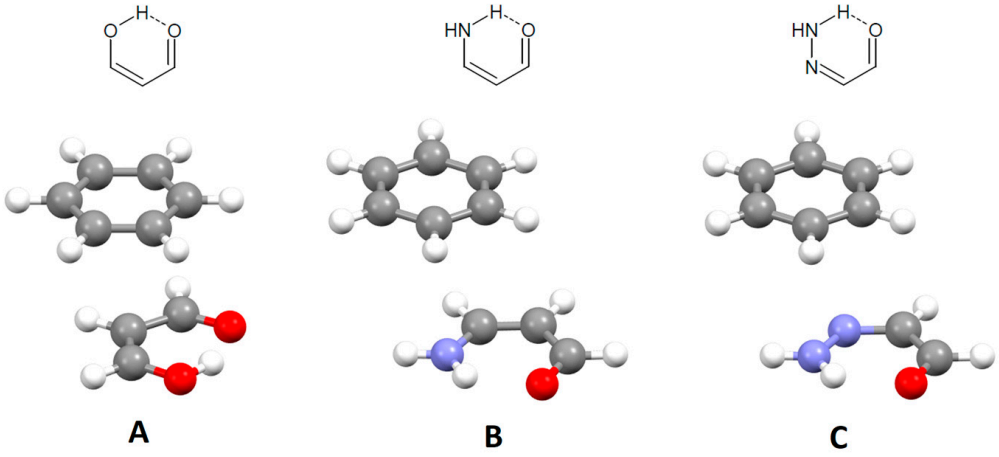

Figure 39. Molecules used for the model systems for quantum chemical calculations of stacking interaction energies between RAHB and aromatic rings were benzene and (2Z)-3-hydroxyprop-2-enal (**A**), (2Z)-3-aminoprop-2-enal (**B**) and (2Z)-hydrazinylideneacetaldehyde (**C**). Presented are the arrangements with strongest stacking interactions for each system. Atom colors: carbon—dark gray, hydrogen—white, nitrogen—blue, oxygen—red.

The SAPT2+3 analysis of the nature of stacking interactions between RAHB rings showed that these interactions are dominated by the strong dispersion component, as well as the strong electrostatic component [9]. Both components are the strongest for the HNCCCO dimer (model system B; Figure 38), which possesses the strongest total interaction energy (Table 6) [9]. The RAHB ring with HNNCCO composition (model system C; Figure 38) has the weakest stacking interaction, since the electrostatic contribution

in this dimer is quite small, and the contribution of dispersion is also smaller than in other systems (Table 6) [9]. The calculations were performed on the most stable structures (Figure 38) with antiparallel orientations; the strong influence of the electrostatic component on the interaction energies indicates importance of electrostatics in the stability of antiparallel orientations.

Table 6. Interaction energies (ΔE, in kcal/mol) calculated at the CCSD(T)/CBS level and normal distances (R, in Å) and offset values (r, in Å) for the most stable RAHB/RAHB (Figure 38) and RAHB/benzene stacking interactions (Figure 39). The total interaction energy for RAHB/RAHB was recalculated at SAPT2+3/cc-pVQZ level of theory (SAPT, in kcal/mol) and decomposed into electrostatic (ELST), exchange (EXCH), induction (IND) and dispersion (DISP) components (all in kcal/mol).

Type of Stacking	RAHB Composition [a]	r	R	ΔE	SAPT	ELST	EXCH	IND	DISP
RAHB/RAHB [66]	HOCCCO (A)	0.5	3.30	−4.26	−4.32	−3.55	+5.92	−0.60	−6.10
	HNCCCO (B)	1.8	3.10	−4.74	−4.81	−4.81	+7.86	−1.12	−6.74
	HNNCCO (C)	1.8	3.35	−2.23	−2.09	−0.89	+3.76	−0.33	−4.64
RAHB/benzene [67]	HOCCCO (A)	1.4	3.4	−3.54					
	HNCCCO (B)	1.8	3.3	−3.47					
	HNNCCO (C)	1.5	3.4	−3.20					

[a] See Figure 38 for RAHB/RAHB and Figure 39 for RAHB/benzene.

The data from crystal structures demonstrate that stacking interactions can exist between the rings that are not closed with covalent bonds, but with intramolecular hydrogen bonds. The calculated interaction energies show that stacking interactions of hydrogen-bridged rings, both single-bond and resonance-assisted, are stronger than stacking interactions between aromatic rings. Interestingly, the strongest interactions are the ones of single-bond hydrogen-bridged rings, which do not possess π-electrons within the rings. The combined crystallographic and computational analysis illustrates that aromaticity or even the presence of a π-system in the ring is not mandatory for strong stacking interactions.

4. Conclusions

Using the data from crystal structures in the Cambridge Structural Database, it is possible to recognize new types of noncovalent interactions. First, it is possible to find the occurrence of interactions in the crystal structures. In addition, it is possible to describe their most common geometrical parameters, and to determine the most common types of species involved in the interactions. These data from crystal structures can be supported with high-level quantum chemical calculations of interaction energies, preferably at a high CCSD(T)/CBS level, which show that the interactions are attractive and provide information on their relative strength, comparing them with other interactions of those or similar systems. In this way, we recognized that two types of nonaromatic rings, namely metal–chelate rings and hydrogen-bridged rings, are capable of forming stacking interactions.

The crystal data showed that chelate rings, most notably in square planar and square pyramidal complexes of Ni, Cu, Pd and Pt, form stacking interactions with aromatic rings (chelate–aryl stacking) and with other chelate rings (chelate–chelate stacking). Chelate–aryl stacking interactions can be intramolecular and intermolecular, and they have the tendency toward parallel-displaced arrangement. Quantum chemical calculations show that, while their strength depends on the metal in the chelate ring, chelate–aryl stacking interactions (−7.56 kcal/mol) are always stronger than aryl–aryl stacking interactions (−2.73 kcal/mol). Even though they are dominated by dispersion, it was shown that chelate–aryl stacking interactions are stronger than aryl–aryl stacking interactions due to electrostatic effects. Chelate–chelate stacking interactions are preferably parallel-displaced, but they can also be in face-to-face arrangement; in both cases, the mutual orientation of

chelate rings is mostly antiparallel. Chelate–chelate stacking interactions can be significantly stronger (−14.58 kcal/mol) than chelate–aryl and particularly aryl–aryl stacking interactions. Chelate–chelate stacking interactions owe their strength to a very pronounced electrostatic component.

Both single-bond hydrogen-bridged (SBHB) and resonance-assisted hydrogen-bridged (RAHB) rings frequently form stacking interactions in the crystal structures, either with aromatic rings (SBHB-aromatic and RAHB-aromatic stacking) or with other hydrogen-bridged rings (SBHB-SBHB and RAHB-RAHB stacking). These stacking interactions are mostly with a parallel-displaced arrangement and, in the case of SBHB-SBHB and RAHB-RAHB stacking, in antiparallel orientation. The calculations show that the strength of all these stacking interactions depends on the ring composition, and that stacking interactions between two hydrogen-bridged rings (−4.89 kcal/mol for SBHB-SBHB and −4.74 kcal/mol for RAHB-RAHB) are somewhat stronger than stacking interactions between a hydrogen-bridged and aromatic ring (−4.38 kcal/mol for SBHB-aromatic and −3.54 kcal/mol for RAHB-aromatic stacking). Both stacking between two hydrogen-bridged rings and stacking of hydrogen-bridged rings with aromatic rings are stronger than aryl–aryl stacking interactions (−2.73 kcal/mol). Stacking interactions of hydrogen-bridged rings are dominated by dispersion, with substantial contribution of electrostatic interactions as well.

The analysis of the crystal data in the CSD supported with quantum chemical calculations shed a light on these new types of stacking interactions, that are very important for the supramolecular systems in which they are found. It was shown how these new types of stacking interactions are able to compete and very often prevail over traditional and more famous types of stacking interactions. Moreover, these studies showed that the crystal data deposited in the Cambridge Structural Database are a powerful tool for studying noncovalent interactions.

Funding: This research was funded by the Ministry of Science, Technological Development and Innovation of Republic of Serbia, contract number: 451-03-47/2023-01/200168.

Data Availability Statement: The data presented in this study are available on request from the corresponding author.

Acknowledgments: The authors express their gratitude for high-performance computing resources to IT Research Computing Group at Texas A&M University in Qatar, which is funded by the Qatar Foundation for Education, Science and Community Development. The authors are also grateful to Dr. Jelena Blagojević Filipović for providing the data on stacking interactions of hydrogen-bridged rings.

Conflicts of Interest: The authors declare no conflict of interest.

References

1. Taylor, R.; Wood, P.A. A Million Crystal Structures: The Whole Is Greater than the Sum of Its Parts. *Chem. Rev.* **2019**, *119*, 9427–9477. [CrossRef] [PubMed]
2. Groom, C.R.; Bruno, I.J.; Lightfoot, M.P.; Ward, S.C. The Cambridge Structural Database. *Acta Crystallogr. B* **2016**, *72*, 171–179. [CrossRef]
3. Malenov, D.P.; Janjić, G.V.; Medaković, V.B.; Hall, M.B.; Zarić, S.D. Noncovalent Bonding: Stacking Interactions of Chelate Rings of Transition Metal Complexes. *Coord. Chem. Rev.* **2017**, *345*, 318–341. [CrossRef]
4. Ninković, D.B.; Janjić, G.V.; Veljković, D.Ž.; Sredojević, D.N.; Zarić, S.D. What Are the Preferred Horizontal Displacements in Parallel Aromatic-Aromatic Interactions? Significant Interactions at Large Displacements. *ChemPhysChem* **2011**, *12*, 3511–3514. [CrossRef]
5. Janjić, G.V.; Veljković, D.Z.; Zarić, S.D.; Janjić, G.V.; Veljković, D.Ž.; Zarić, S.D. Water/Aromatic Parallel Alignment Interactions. Significant Interactions at Large Horizontal Displacements. *Cryst. Growth Des.* **2011**, *11*, 2680–2683. [CrossRef]
6. Milovanović, M.R.; Stanković, I.M.; Živković, J.M.; Ninković, D.B.; Hall, M.B.; Zarić, S.D. Water: New Aspect of Hydrogen Bonding in the Solid State. *IUCrJ* **2022**, *9*, 639–647. [CrossRef]
7. Blagojević, J.P.; Zarić, S.D. Stacking Interactions of Hydrogen-Bridged Rings—Stronger than the Stacking of Benzene Molecules. *Chem. Commun.* **2015**, *51*, 12989–12991. [CrossRef]
8. Blagojević, J.P.; Veljković, D.Ž.; Zarić, S.D. Stacking Interactions between Hydrogen-Bridged and Aromatic Rings: Study of Crystal Structures and Quantum Chemical Calculations. *CrystEngComm* **2017**, *19*, 40–46. [CrossRef]

9. Blagojević Filipović, J.P.; Hall, M.B.; Zarić, S.D. Stacking Interactions of Resonance-Assisted Hydrogen-Bridged Rings. A Systematic Study of Crystal Structures and Quantum-Chemical Calculations. *Cryst. Growth Des.* **2019**, *19*, 5619–5628. [CrossRef]
10. Blagojević Filipović, J.P.; Hall, M.B.; Zarić, S.D. Stacking Interactions of Resonance-Assisted Hydrogen-Bridged Rings and C6-Aromatic Rings. *Phys. Chem. Chem. Phys.* **2020**, *22*, 13721–13728. [CrossRef]
11. Bogdanović, G.A.; Biré, A.S.; Zarić, S.D. Evidence Based on Crystal Structures and Calculations of a C−H···π Interaction Between an Organic Moiety and a Chelate Ring in Transition Metal Complexes. *Eur. J. Inorg. Chem.* **2002**, *2002*, 1599–1602. [CrossRef]
12. Yakovchuk, P.; Protozanova, E.; Frank-Kamenetskii, M.D. Base-Stacking and Base-Pairing Contributions into Thermal Stability of the DNA Double Helix. *Nucleic Acids Res.* **2006**, *34*, 564–574. [CrossRef] [PubMed]
13. Balakrishnan, S.; Sarma, S.P. Engineering Aromatic–Aromatic Interactions To Nucleate Folding in Intrinsically Disordered Regions of Proteins. *Biochemistry* **2017**, *56*, 4346–4359. [CrossRef] [PubMed]
14. Zhuang, W.-R.; Wang, Y.; Cui, P.-F.; Xing, L.; Lee, J.; Kim, D.; Jiang, H.-L.; Oh, Y.-K. Applications of π-π Stacking Interactions in the Design of Drug-Delivery Systems. *J. Control Release* **2019**, *294*, 311–326. [CrossRef]
15. Ahmed, E.; Karothu, D.P.; Naumov, P. Crystal Adaptronics: Mechanically Reconfigurable Elastic and Superelastic Molecular Crystals. *Angew. Chem. Int. Ed.* **2018**, *57*, 8837–8846. [CrossRef]
16. Chen, T.; Li, M.; Liu, J. π–π Stacking Interaction: A Nondestructive and Facile Means in Material Engineering for Bioapplications. *Cryst. Growth Des.* **2018**, *18*, 2765–2783. [CrossRef]
17. Bludský, O.; Rubeš, M.; Soldán, P.; Nachtigall, P. Investigation of the Benzene-Dimer Potential Energy Surface: DFT/CCSD(T) Correction Scheme. *J. Chem. Phys.* **2008**, *128*, 114102. [CrossRef]
18. Lee, E.C.; Kim, D.; Jurečka, P.; Tarakeshwar, P.; Hobza, P.; Kim, K.S. Understanding of Assembly Phenomena by Aromatic−Aromatic Interactions: Benzene Dimer and the Substituted Systems. *J. Phys. Chem. A* **2007**, *111*, 3446–3457. [CrossRef]
19. Bettinger, H.F.; Kar, T.; Sánchez-García, E.; Sánchez-García, E. Borazine and Benzene Homo- And Heterodimers. *J. Phys. Chem. A* **2009**, *113*, 3353–3359. [CrossRef]
20. Pitoňák, M.; Neogrády, P.; Řezáč, J.; Jurečka, P.; Urban, M.; Hobza, P. Benzene Dimer: High-Level Wave Function and Density Functional Theory Calculations. *J. Chem. Theory Comput.* **2008**, *4*, 1829–1834. [CrossRef]
21. Grimme, S. Do Special Noncovalent π-π Stacking Interactions Really Exist? *Angew. Chem. Int. Ed.* **2008**, *47*, 3430–3434. [CrossRef] [PubMed]
22. Bloom, J.W.G.; Wheeler, S.E. Taking the Aromaticity out of Aromatic Interactions. *Angew. Chem. Int. Ed.* **2011**, *50*, 7847–7849. [CrossRef] [PubMed]
23. Tomic, Z.D.; Leovac, V.M.; Pokorni, S.V.; Zobel, D.; Zaric, S.D. Crystal Structure of Bis[Acetone-1-Naphthoylhydrazinato(-1)]Copper(II) and Investigations of Intermolecular Interactions. *Eur. J. Inorg. Chem.* **2003**, *2003*, 1222–1226. [CrossRef]
24. Castiñeiras, A.; Sicilia-Zafra, A.G.; González-Pérez, J.M.; Choquesillo-Lazarte, D.; Niclós-Gutiérrez, J. Intramolecular "Aryl−Metal Chelate Ring" π,π-Interactions as Structural Evidence for Metalloaromaticity in (Aromatic α,α′-Diimine)−Copper(II) Chelates: Molecular and Crystal Structure of Aqua(1,10-Phenanthroline)(2-Benzylmalonato)Copper(II) Three-Hydrate. *Inorg. Chem.* **2002**, *41*, 6956–6958. [CrossRef] [PubMed]
25. Milčić, M.K.; Ostojić, B.D.; Zarić, S.D. Are Chelate Rings Aromatic? Calculations of Magnetic Properties of Acetylacetonato and o -Benzoquinonediimine Chelate Rings. *Inorg. Chem.* **2007**, *46*, 7109–7114. [CrossRef]
26. Tomić, Z.D.; Novaković, S.B.; Zarić, S.D. Intermolecular Interactions between Chelate Rings and Phenyl Rings in Square-Planar Copper(II) Complexes. *Eur. J. Inorg. Chem.* **2004**, 2215–2218. [CrossRef]
27. Tomić, Z.D.; Sredojević, D.; Zarić, S.D. Stacking Interactions between Chelate and Phenyl Rings in Square-Planar Transition Metal Complexes. *Cryst. Growth Des.* **2006**, *6*, 29–31. [CrossRef]
28. Sredojević, D.N.; Tomić, Z.D.; Zarić, S.D. Influence of Metal and Ligand Types on Stacking Interactions of Phenyl Rings with Square-Planar Transition Metal Complexes. *Cent. Eur. J. Chem.* **2007**, *5*, 20–31. [CrossRef]
29. Yang, X.-J.; Drepper, F.; Wu, B.; Sun, W.-H.; Haehnel, W.; Janiak, C. From Model Compounds to Protein Binding: Syntheses, Characterizations and Fluorescence Studies of [Ru II (Bipy)(Terpy)L] 2+ Complexes (Bipy = 2,2′-Bipyridine; Terpy = 2,2′:6′,2″-Terpyridine; L = Imidazole, Pyrazole and Derivatives, Cytochrome C). *Dalt. Trans.* **2005**, 256–267. [CrossRef]
30. Mosae Selvakumar, P.; Suresh, E.; Subramanian, P.S. Single Stranded Helical Supramolecular Architecture with a Left Handed Helical Water Chain in Ternary Copper(II) Tryptophan/Diamine Complexes. *Polyhedron* **2009**, *28*, 245–252. [CrossRef]
31. Allali, M.; Jaud, J.; Habbadi, N.; Dartiguenave, M.; Beauchamp, A.L.; Benoist, E. Structural Evidence for an Unusual Conformation and Weak Interligand Interactions in Two Copper Chelates with (o-Nitrophenyl)-Ethylenediaminediacetic Acid. *Eur. J. Inorg. Chem.* **2009**, *2009*, 1488–1494. [CrossRef]
32. Philip, V.; Suni, V.; Prathapachandra Kurup, M.R.; Nethaji, M. Structural and Spectral Studies of Nickel(II) Complexes of Di-2-Pyridyl Ketone N4,N4-(Butane-1,4-Diyl) Thiosemicarbazone. *Polyhedron* **2004**, *23*, 1225–1233. [CrossRef]
33. Sredojević, D.N.; Vojislavljević, D.Z.; Tomić, Z.D.; Zarić, S.D. Parallel Stacking Interactions in Square-Planar Transition-Metal Complexes Containing Fused Chelate and C6-Aromatic Rings. *Acta Crystallogr. B* **2012**, *68*, 261–265. [CrossRef]
34. Malenov, D.P.; Ninković, D.B.; Sredojević, D.N.; Zarić, S.D. Stacking of Benzene with Metal Chelates: Calculated CCSD(T)/CBS Interaction Energies and Potential-Energy Curves. *ChemPhysChem* **2014**, *15*, 2458–2461. [CrossRef] [PubMed]
35. Malenov, D.P.; Ninković, D.B.; Zarić, S.D. Stacking of Metal Chelates with Benzene: Can Dispersion-Corrected DFT Be Used to Calculate Organic-Inorganic Stacking? *ChemPhysChem* **2015**, *16*, 761–768. [CrossRef]

36. Malenov, D.P.; Hall, M.B.; Zarić, S.D. Influence of Metal Ion on Chelate-Aryl Stacking Interactions. *Int. J. Quantum Chem.* **2018**, *118*, e25629. [CrossRef]
37. Malenov, D.P.; Veljković, D.Ž.; Hall, M.B.; Brothers, E.N.; Zarić, S.D. Influence of Chelate Ring Type on Chelate–Chelate and Chelate–Aryl Stacking: The Case of Nickel Bis(Dithiolene). *Phys. Chem. Chem. Phys.* **2019**, *21*, 1198–1206. [CrossRef]
38. Malenov, D.P.; Zarić, S.D. Strong Stacking Interactions of Metal–Chelate Rings Are Caused by Substantial Electrostatic Component. *Dalton Trans.* **2019**, *48*, 6328–6332. [CrossRef]
39. Sredojević, D.N.; Ninković, D.B.; Janjić, G.V.; Zhou, J.; Hall, M.B.; Zarić, S.D. Stacking Interactions of Ni(Acac) Chelates with Benzene: Calculated Interaction Energies. *ChemPhysChem* **2013**, *14*, 1797–1800. [CrossRef]
40. MacKie, I.D.; DiLabio, G.A. Approximations to Complete Basis Set-Extrapolated, Highly Correlated Non-Covalent Interaction Energies. *J. Chem. Phys.* **2011**, *135*, 134318. [CrossRef]
41. Jeziorski, B.; Moszynski, R.; Szalewicz, K. Perturbation Theory Approach to Intermolecular Potential Energy Surfaces of van Der Waals Complexes. *Chem. Rev.* **1994**, *94*, 1887–1930. [CrossRef]
42. Hohenstein, E.G.; Sherrill, C.D. Density Fitting and Cholesky Decomposition Approximations in Symmetry-Adapted Perturbation Theory: Implementation and Application to Probe the Nature of π-π Interactions in Linear Acenes. *J. Chem. Phys.* **2010**, *132*, 184111. [CrossRef]
43. Gonthier, J.F.; Sherrill, C.D. Density-Fitted Open-Shell Symmetry-Adapted Perturbation Theory and Application to π -Stacking in Benzene Dimer Cation and Ionized DNA Base Pair Steps. *J. Chem. Phys.* **2016**, *145*, 134106. [CrossRef] [PubMed]
44. Hohenstein, E.G.; Sherrill, C.D. Effects of Heteroatoms on Aromatic π-π Interactions: Benzene-Pyridine and Pyridine Dimer. *J. Phys. Chem. A* **2009**, *113*, 878–886. [CrossRef]
45. Ninković, D.B.; Blagojević Filipović, J.P.; Hall, M.B.; Brothers, E.N.; Zarić, S.D. What Is Special about Aromatic-Aromatic Interactions? Significant Attraction at Large Horizontal Displacement. *ACS Cent. Sci.* **2020**, *6*, 420–425. [CrossRef]
46. Janiak, C. A Critical Account on π-π Stacking in Metal Complexes with Aromatic Nitrogen-Containing Ligands. *J. Chem. Soc. Dalton Trans.* **2000**, *95*, 3885–3896. [CrossRef]
47. Sredojević, D.N.; Tomić, Z.D.; Zarić, S.D. Evidence of Chelate-Chelate Stacking Interactions in Crystal Structures of Transition-Metal Complexes. *Cryst. Growth Des.* **2010**, *10*, 3901–3908. [CrossRef]
48. Brock, A.J.; Whittaker, J.J.; Powell, J.A.; Pfrunder, M.C.; Grosjean, A.; Parsons, S.; McMurtrie, J.C.; Clegg, J.K. Elastically Flexible Crystals Have Disparate Mechanisms of Molecular Movement Induced by Strain and Heat. *Angew. Chem. Int. Ed.* **2018**, *57*, 11325–11328. [CrossRef]
49. Joksimović, N.; Janković, N.; Petronijević, J.; Baskić, D.; Popovic, S.; Todorović, D.; Zarić, M.; Klisurić, O.; Vraneš, M.; Tot, A.; et al. Synthesis, Anticancer Evaluation and Synergistic Effects with Cis Platin of Novel Palladium Complexes: DNA, BSA Interactions and Molecular Docking Study. *Med. Chem.* **2020**, *16*, 78–92. [CrossRef]
50. Mahmoudi, G.; Castiñeiras, A.; Garczarek, P.; Bauzá, A.; Rheingold, A.L.; Kinzhybalo, V.; Frontera, A. Synthesis, X-Ray Characterization, DFT Calculations and Hirshfeld Surface Analysis of Thiosemicarbazone Complexes of Mn+ Ions (n = 2, 3; M = Ni, Cd, Mn, Co and Cu). *CrystEngComm* **2016**, *18*, 1009–1023. [CrossRef]
51. Holland, L.; Shen, W.Z.; Von Grebe, P.; Sanz Miguel, P.J.; Pichierri, F.; Springer, A.; Schalley, C.A.; Lippert, B. A Neutral Pt 3 Stack Unsupported by Any Bridging Ligand. *Dalton Trans.* **2011**, *40*, 5159–5161. [CrossRef] [PubMed]
52. Laurila, E.; Oresmaa, L.; Niskanen, M.; Hirva, P.; Haukka, M. Metal−Metal Interactions in Stacked Mononuclear and Dinuclear Rhodium 2,2′-Biimidazole Carbonyl Complexes. *Cryst. Growth Des.* **2010**, *10*, 3775–3786. [CrossRef]
53. Hosseini-Monfared, H.; Pousaneh, E.; Sadighian, S.; Ng, S.W.; Tiekink, E.R.T.T. Syntheses, Structures, and Catalytic Activity of Copper(II)-Aroylhydrazone Complexes. *Z. Anorg. Allg. Chem.* **2013**, *639*, 435–442. [CrossRef]
54. Malenov, D.P.; Zarić, S.D. Chelated Metal Ions Modulate the Strength and Geometry of Stacking Interactions: Energies and Potential Energy Surfaces for Chelate–Chelate Stacking. *Phys. Chem. Chem. Phys.* **2018**, *20*, 14053–14060. [CrossRef] [PubMed]
55. Gilli, G.; Bellucci, F.; Ferretti, V.; Bertolasi, V. Evidence for Resonance-Assisted Hydrogen Bonding from Crystal-Structure Correlations on the Enol Form of the .Beta.-Diketone Fragment. *J. Am. Chem. Soc.* **1989**, *111*, 1023–1028. [CrossRef]
56. Gilli, P.; Bertolasi, V.; Ferretti, V.; Gilli, G. Evidence for Intramolecular N-H···O Resonance-Assisted Hydrogen Bonding in β-Enaminones and Related Heterodienes. A Combined Crystal-Structural, IR and NMR Spectroscopic, and Quantum-Mechanical Investigation. *J. Am. Chem. Soc.* **2000**, *122*, 10405–10417. [CrossRef]
57. Mahmudov, K.T.; Pombeiro, A.J.L. Resonance-Assisted Hydrogen Bonding as a Driving Force in Synthesis and a Synthon in the Design of Materials. *Chem. Eur. J.* **2016**, *22*, 16356–16398. [CrossRef]
58. Shapenova, D.S.; Shiryaev, A.A.; Bolte, M.; Kukułka, M.; Szczepanik, D.W.; Hooper, J.; Babashkina, M.G.; Mahmoudi, G.; Mitoraj, M.P.; Safin, D.A. Resonance Assisted Hydrogen Bonding Phenomenon Unveiled through Both Experiments and Theory: A New Family of Ethyl N-Salicylideneglycinate Dyes. *Chem. Eur. J.* **2020**, *26*, 12987–12995. [CrossRef]
59. Sanz, P.; Mó, O.; Yáñez, M.; Elguero, J. Resonance-Assisted Hydrogen Bonds: A Critical Examination. Structure and Stability of the Enols of β-Diketones and β-Enaminones. *J. Phys. Chem. A* **2007**, *111*, 3585–3591. [CrossRef]
60. Jabłoński, M.; Kaczmarek, A.; Sadlej, A.J. Estimates of the Energy of Intramolecular Hydrogen Bonds. *J. Phys. Chem. A* **2006**, *110*, 10890–10898. [CrossRef]
61. Mason, P.E.; Dempsey, C.E.; Neilson, G.W.; Kline, S.R.; Brady, J.W. Preferential Interactions of Guanidinum Ions with Aromatic Groups over Aliphatic Groups. *J. Am. Chem. Soc.* **2009**, *131*, 16689–16696. [CrossRef] [PubMed]

62. Negi, I.; Jangra, R.; Gharu, A.; Trant, J.F.; Sharma, P. Guanidinium–Amino Acid Hydrogen-Bonding Interactions in Protein Crystal Structures: Implications for Guanidinium-Induced Protein Denaturation. *Phys. Chem. Chem. Phys.* **2022**, *25*, 857–869. [CrossRef] [PubMed]
63. Prabhakar, A.S.; Sashikanth, S.; Reddy, P.P.; Cherukupally, P. An Efficient Synthesis of Vinylogous Carbamates from Alkyl Azides. *Tetrahedron Lett.* **2007**, *48*, 8709–8711. [CrossRef]
64. Mahmudov, K.T.; Kopylovich, M.N.; Guedes da Silva, M.F.C.; Pombeiro, A.J.L. Interplay between Resonance-Assisted Hydrogen Bonding and Coordination in Sulfo-Functionalized Arylhydrazones of Active Methylene Compounds. *Chempluschem* **2014**, *79*, 1523–1531. [CrossRef]
65. Saccone, M.; Pfletscher, M.; Kather, S.; Wölper, C.; Daniliuc, C.; Mezger, M.; Giese, M. Improving the Mesomorphic Behaviour of Supramolecular Liquid Crystals by Resonance-Assisted Hydrogen Bonding. *J. Mater. Chem. C* **2019**, *7*, 8643–8648. [CrossRef]
66. Vetrichelvan, M.; Valiyaveettil, S. Intramolecular Hydrogen-Bond-Assisted Planarization of Asymmetrically Functionalized Alternating Phenylene-Pyridinylene Copolymers. *Chem. Eur. J.* **2005**, *11*, 5889–5898. [CrossRef]
67. Blagojević, J.; Janjić, G.; Zarić, S. Very Strong Parallel Interactions Between Two Saturated Acyclic Groups Closed with Intramolecular Hydrogen Bonds Forming Hydrogen-Bridged Rings. *Crystals* **2016**, *6*, 34. [CrossRef]
68. Filipović, J.P.B.; Zarić, S.D. Significant Stacking Interactions of Resonance-Assisted Hydrogen-Bridged (RAHB) Rings at Large Horizontal Displacements. *Cryst. Growth Des.* **2021**, *21*, 4947–4958. [CrossRef]
69. Lobana, T.S.; Sharma, R.; Castineiras, A.; Hundal, G.; Butcher, R.J. The Influence of Substituents (R) at N1 Atom of Thiophene-2-Carbaldehyde Thiosemicarbazones {(C4H3S)HC2N3–N(H)–C1(S)N1HR} on Bonding, Nuclearity and H-Bonded Networks of Copper(I) Complexes. *Inorg. Chim. Acta* **2009**, *362*, 3547–3554. [CrossRef]
70. Saravanan, S.; Muthusubramanian, S. {3-[4-(N,N-Dimethylamino)Phenyl]-1-(4-Methylphenyl)-3-(Phenylsulfanyl)Propylidene}semicarbazide. *Acta Crystallogr. E* **2004**, *60*, o1895–o1897. [CrossRef]
71. Carballo, R.; Pino-Cuevas, A.; Vázquez-López, E.M. Crystal Structure of 1-(4-Formylbenzylidene)Thiosemicarbazone. *Acta Crystallogr. E* **2014**, *70*, o970. [CrossRef] [PubMed]
72. Ma, N.; Wang, Y.; Ji, B.-M. Crystal Structure of Pyridine-2-Carbaldehyde Thiosemicarbazonium Chloride Hydrate, $[C7H9N4S]Cl \cdot H_2O$. *Z. Kristallogr. NCS* **2011**, *226*, 463–464. [CrossRef]
73. Hohenstein, E.G.; Sherrill, C.D. Density Fitting of Intramonomer Correlation Effects in Symmetry-Adapted Perturbation Theory. *J. Chem. Phys.* **2010**, *133*, 014101. [CrossRef] [PubMed]
74. Hansen, F.; Hazell, R.G.; Larsen, C.; Nielsen, P.H.; Lindberg, A.A.; Jansen, G.; Lamm, B.; Samuelsson, B. The Crystal Structure of Thiosemicarbazide. *Acta Chem. Scand.* **1969**, *23*, 1359–1366. [CrossRef]
75. Xu, L.-X.; Bai, X.-G.; Wang, J.-X.; Wang, Y.-C. (Z)-Methyl 3-(2,4-Dichlorophenyl)-3-Hydroxyacrylate. *Acta Crystallogr. E* **2012**, *68*, o4. [CrossRef]
76. Ostrowska, K.; Musielak, B.; Szneler, E.; Dudek, Ł.; Gryl, M.; Stadnicka, K. Chelate Ring Size Effect as a Factor of Selective Fluorescent Recognition of Zn 2+ Ions by Pyrrolo[2,3-b]Quinoxaline with a Substituted 2-Pyridyl Group Receptor. *Inorg. Chem.* **2015**, *54*, 8423–8435. [CrossRef]
77. Alpaslan, G.; Özdamar, Ö.; Odabaşoğlu, M.; Ocak Ískeleli, N.; Erdönmez, A. (Z)-Ethyl 2-[2-(4-Acetylphenyl)Hydrazono]-4-Chloro-3-Oxobutanoate. *Acta Crystallogr. E* **2007**, *63*, o2746. [CrossRef]
78. Rojas, R.S.; Cabrera, A.R.; Peoples, B.C.; Spannhoff, K.; Valderrama, M.; Fröhlich, R.; Kehr, G.; Erker, G. Synthesis of [(π-Cyano-P-Nacnac)Cp] and [(π-Cyano-Nacnac)Cp]-Zirconium Complexes, and Their Remote Activation for Ethylene Polymerization. *Dalton Trans.* **2012**, *41*, 1243–1251. [CrossRef]